Integrated systems biology identifies disruptions in mitochondrial function and metabolism as key contributors to heart failure with preserved ejection fraction (HFpEF)

Andrew A. Gibb, PhD[a,c*], Kyle LaPenna, MD, PhD[b], Ryan B. Gaspar, BS[c], Nadina R. Latchman, BS[c], Yinfei Tan, PhD[d], Carmen Choya-Foces, PhD[c], Jake E. Doiron, PhD[b], Zhen Li, PhD[e], Huijing Xia, PhD[b], Michael P. Lazaropoulos, PhD[c], Mariell Conwell, BS[c], Thomas E. Sharp III, PhD[f], Traci T. Goodchild, PhD[e], David J. Lefer, PhD[e*], John W. Elrod, PhD[c*]

[a]Center for Cardiometabolic Science, Christina Lee Brown Envirome Institute, Department of Medicine, University of Louisville, Louisville, KY, USA
[b]Cardiovascular Center for Excellence, Department of Pharmacology, Louisiana State University Health Science Center, New Orleans, LA, USA
[c]Aging + Cardiovascular Discovery Center, Department of Cardiovascular Sciences, Lewis Katz School of Medicine, Temple University, Philadelphia, PA, USA
[d]Fox Chase Cancer Center, Temple University, Philadelphia, PA, USA
[e]Smidt Heart Institute, Cedars-Sinai Medical Center, Los Angeles, CA, USA
[f]Department of Molecular Pharmacology and Physiology, University of South Florida Health, Tampa, FL, USA

*Co-corresponding authors

John W. Elrod, PhD
elrod@temple.edu

or

David J. Lefer, PhD
david.lefer@cshs.org

or

Andrew A. Gibb, PhD
andrew.gibb@louisville.edu

Running Title:

Mitochondrial Metabolism in HFpEF Development

ABSTRACT

Background: Heart failure with preserved ejection fraction (HFpEF) accounts for ~50% of HF cases, with no effective treatments. The ZSF1-obese rat model recapitulates numerous clinical features of HFpEF including hypertension, obesity, metabolic syndrome, exercise intolerance, and LV diastolic dysfunction. Here, we utilized a systems-biology approach to define the early metabolic and transcriptional signatures to gain mechanistic insight into the pathways contributing to HFpEF development.

Methods: Male ZSF1-obese, ZSF1-lean hypertensive controls, and WKY (wild-type) controls were compared at 14w of age for extensive physiological phenotyping and LV tissue harvesting for unbiased metabolomics, RNA-sequencing, and assessment of mitochondrial morphology and function. Utilizing ZSF1-lean and WKY controls enabled a distinction between hypertension-driven molecular changes contributing to HFpEF pathology, versus hypertension + metabolic syndrome.

Results: ZSF1-obese rats displayed numerous clinical features of HFpEF. Comparison of ZSF1-lean vs WKY (i.e., hypertension-exclusive effects) revealed metabolic remodeling suggestive of increased aerobic glycolysis, decreased β-oxidation, and dysregulated purine and pyrimidine metabolism with few transcriptional changes. ZSF1-obese rats displayed worsened metabolic remodeling and robust transcriptional remodeling highlighted by the upregulation of inflammatory genes and downregulation of the mitochondrial structure/function and cellular metabolic processes. Integrated network analysis of metabolomic and RNAseq datasets revealed downregulation of nearly all catabolic pathways contributing to energy production, manifesting in a marked decrease in the energetic state (i.e., reduced ATP/ADP, PCr/ATP). Cardiomyocyte

ultrastructure analysis revealed decreased mitochondrial area, size, and cristae density, as well as increased lipid droplet content in HFpEF hearts. Mitochondrial function was also impaired as demonstrated by decreased substrate-mediated respiration and dysregulated calcium handling.

Conclusions: Collectively, the integrated omics approach applied here provides a framework to uncover novel genes, metabolites, and pathways underlying HFpEF, with an emphasis on mitochondrial energy metabolism as a potential target for intervention.

INTRODUCTION

Heart failure (HF) is a growing epidemic. In the U.S. alone, >6.7 million people over the age of 20 have HF and this is projected to increase to >8.5 million people by 2030[1,2]. Nearly one-quarter of people will develop HF in their lifetime[1-3] and current HF mortality rates are higher today than in 1999[4]. Of those diagnosed with HF, ~50% have heart failure with preserved ejection fraction (HFpEF)[1-3,5]. HFpEF patients present with elevated left ventricular (LV) filling pressure despite normal LV ejection fraction (≥50%). At present there are very limited treatments for HFpEF, and the 5-year mortality rate is merely 50%[1-3]. Clinical trials of drugs that are effective in HF with reduced ejection fraction (HFrEF) have uniformly failed in HFpEF[1,3]. Due to our limited understanding of mechanisms which drive HFpEF and lack of therapeutic strategies to treat this devastating disease, the NIH-NHLBI has issued a statement of emphasis detailing the research priority of HFpEF and identified HFpEF as the greatest unmet need in cardiovascular medicine[6].

While clinicians struggle to treat HFpEF patients, research scientists have grappled with preclinical models to study the pathobiology of HFpEF[7-12] to improve our understanding of this complex, multi-organ disease. Clinically relevant models are required to fully elucidate molecular disease mechanisms and effectively translate new therapies from bench to bedside. Towards this end, the (ZSF1) rat has been proposed as an animal model for HFpEF[13,14]. This model was created by crossing rat strains with two separate leptin receptor mutations (fa and facp), the lean female Zucker diabetic fatty (ZDF) rat (+/fa) and the lean male spontaneously hypertensive heart failure (SHHF) rat. Offspring

homozygous for both mutations (fa:facp) create a hybrid rat with central obesity and hypertension (ZSF1-Obese rat) resulting in spontaneous cardiometabolic HFpEF whereas the heterozygous lean offspring (ZSF1-Lean rat) exhibit no signs of obesity and diabetes[15]. Previous studies have shown that obese ZSF1 rats develop significant diastolic dysfunction between 10-20 weeks of age with concentric LV remodeling and hypertrophy like that observed in HFpEF patients[16]. In addition to LV diastolic dysfunction, previous studies have demonstrated skeletal muscle pathology, exercise intolerance, endothelial dysfunction, systemic inflammation, and renal and hepatic abnormalities that are consistent with cardiometabolic HFpEF[13,16-19]. We have previously demonstrated that the ZSF1 rat is responsive to therapeutic interventions when delivered early during the progression of HFpEF[18,19]. The severity of HFpEF in terms of cardiometabolic pathology has been shown to be similar between male and female ZSF1 obese rats[20], which is not the case for the popular "two-hit" mouse model of HFpEF in which female mice are protected against the development of HFpEF[21]. In summary, the ZSF1 obese rat represents a clinically-relevant and superior model for the elucidation of novel mechanisms responsible for the development and progression of HFpEF.

To uncover potentially novel and critical mechanisms in HFpEF, we provide an in-depth characterization the ZSF1 obese rat model of HFpEF using several physiological, biochemical, molecular, and omics approaches. We evaluated male ZSF1-obese, ZSF1-lean hypertensive controls, and WKY (wild-type) lean, normotensive controls at an early stage in the development of HFpEF (14-wks of age), performing extensive

physiological phenotyping in conjunction with unbiased metabolomics and transcriptomics. Our results reveal that the addition of obesity/metabolic syndrome upon hypertension and vascular dysfunction is a primary contributor to gross cardiac transcriptional and metabolic remodeling, driving the development of HFpEF. Most notably, mitochondrial energy metabolism pathways were highly disrupted resulting in an energetic deficit that correlated with maladaptive mitochondrial ultrastructural remodeling and functional impairment. These findings support an integrated framework to identify metabolic and transcriptional pathways that are disrupted in, and contribute to, HFpEF progression that will optimally yield new therapeutic targets.

METHODS

Experimental Animals: Wistar Kyoto (WKY), ZSF1-lean, and ZSF1-obese male rats were purchased from Charles River laboratories and used in all experiments contained within this study (n=5 to 7 per group). Animals were purchased and held at Temple University Lewis Katz School of Medicine (TU-LKSOM) or LSU Health Sciences Center (LSUHSC) in a temperature controlled and 12-hour light/dark cycle for the entirety of studies. All studies were approved by TU-LKSOM and LSUHSC Institutional Animal Care and Use Committees (IACUC) and received animal care at TU-LKSOM and LSUHSC according to the Association for Assessment and Accreditation of Laboratory Animal International (AAALAC) guidelines.

Study Design: Both ZSF1-lean, ZSF1-obese, and WKY controls were investigated at 14 wks of age. Physiologic parameters of body weight, transthoracic echocardiography, and exercise capacity testing are as described below. Further investigation into pathophysiology of these separate animal models was performed utilizing left ventricular (LV) and systemic invasive hemodynamic measurements along with ex vivo assessments of mitochondrial ultrastructure and function. Isolated cardiac LV tissue samples were also submitted for RNAseq and unbiased metabolomics.

Echocardiography: Transthoracic echocardiography of all groups was performed with a Vevo 2100 echocardiography system (FUJIFILM VisualSonics). Left ventricular diastolic measurements were performed using an apical four chambered view of the heart. Left ventricular systolic measurements were performed using a long-axis view. Animals were

anesthetized using inhaled isoflurane at an induction dose of 3% with a maintenance dose of 1% for the longevity of the experiment. Heart rate was maintained at approximately 250-300 beats per minute (BPM) for the data collection period as previously described[22].

Exercise Capacity Testing: ZSF1-lean, ZSF1-obese, and WKY control rats were assessed for exercise intolerance utilizing a IITC Life Science 800 Series treadmill. Animals were first acclimated to the treadmill for a period of 5 minutes with no movement, they were then brought through a warmup phase consisting of initially 6 meters per minute which was thereby increased to 12 meters per minute for a 4-minute ramp up time, for a total warmup phase of 5 minutes. For data collection as presented, the animals were run at a rate of 12 meters per minute with 0° incline until exhaustion, which was defined as animal placement on the shock pads for more than 3 seconds. Exercise capacity was then determined by the total distance run.

Terminal Invasive Hemodynamics and Sacrifice: At 14 wks of age, animals were anesthetized via inhaled isoflurane at a concentration of 3% for induction and 1% maintenance during the following procedure. The rodent neck and associated structures were dissected for exposure of the common carotid which was canulated with a 1.2 F high-fidelity pressure catheter, measuring the systemic pressures at systole and diastole accordingly for multiple cardiac cycles. The pressure catheter was then carefully introduced into the left ventricle of the animal. Left ventricular end diastolic pressures (LVEDP) and ventricular relaxation time constant (Tau) were measured after multiple

178 cardiac cycles to obtain an average measurement. The catheter was then removed, and
179 the rat was subsequently exsanguinated and sacrificed with tissues and plasma
180 harvested for additional measurements as previously described[23].
181
182 *Mitochondrial function*: Heart mitochondria were isolated and subjected to respiratory
183 function assays using the Seahorse XF96, like that described previously[7,24]. Briefly,
184 ~100 mg left ventricular heart pieces were washed 5× with cold buffer A (220 mM
185 mannitol, 70 mM sucrose, 5 mM MOPS, 1 mM EDTA; pH 7.2 with KOH) followed by
186 homogenization using a glass-col homogenizer in 2 ml of buffer A containing 0.2% fatty
187 acid-free BSA. Homogenate was then subjected to centrifugation at 800 × *g* for 10 min
188 followed by supernatant collection and centrifugation at 10,000 × *g* for 10 min. The
189 pellet containing mitochondria was then resuspended in 1 ml fresh buffer A (without
190 BSA) and centrifuged at 10,000 × *g*, with this step repeated once. The washed
191 mitochondrial pellet was then resuspended in 150 µl respiration buffer (120 mM KCl, 25
192 mM Sucrose, 10 mM HEPES, 1 mM $MgCl_2$, 5 mM KH_2PO_4; pH 7.2 with KOH) and kept
193 on ice.
194 To determine mitochondrial function, samples were diluted to a concentration of
195 2.5 µg (protein) in 50 µl respiration buffer per well and centrifuged onto XF96
196 microplates at 500 × *g* for 3 min at 4°C. State 3 respiration in response to substrates
197 were measured after injection of pyruvate + malate (5.0 mM + 2.5 mM, final
198 concentrations) or succinate + rotenone (10 mM + 1 µM, final concentrations) to assess
199 complex I and II rates, respectively. Fatty acid oxidation was assessed in response to
200 palmitoyl-l-carnitine + malate (50 µM + 2.5 mM, final concentration). The oxygen

consumption rates recorded after injection of oligomycin (1 µg/ml), an inhibitor of ATP synthase, served as a measure of State 4 respiration. Following State 4 respiratory measurements, injection of FCCP, a mitochondrial uncoupler, provided ETC complex maximal respiratory capacity. Respiratory control ratios, state 3/state 4, were calculated as a measure of the coupling of oxygen consumption to ATP production.

Mitochondrial calcium uptake assay: Isolated mitochondria were diluted in Isolated Mitochondria Assay Buffer (IMAB; 125 mM KCl, 10 mM NaCl, 20 mM HEPES, 2 mM $MgCl_2$, 2 mM KH_2PO_4, pH 7.2 with KOH). Mitochondria were loaded into 96-well plates (final concentration of 1 µg/µL), supplemented with 10 mM succinate (Sigma-Aldrich, S3674), 10 mM malate (Sigma-Aldrich, 240176) and 10 mM pyruvate (Sigma-Aldrich, P5280), and 1 µM calcium green-5N hexapotassium salt (Invitrogen, C-3737). Final volume at the start of the assay was 50 µL. Fluorescence was measured every 200 ms at 506 nm_{ex}/532 nm_{em} using a TECAN Infinite M1000 Pro plate reader set at 37°C. After 120 sec of baseline measurements, successive injections of 2.5 µM $CaCl_2$ (5 µL of 25 µM $CaCl_2$ stock prepared in IMAB) were administered every 120 sec. To generate a standard curve of extramitochondrial Ca^{2+} (bath concentration), the same experimental setup was employed without addition of mitochondria to the well. The standard curve was utilized to calculate the extramitochondrial calcium remaining post mitochondrial uptake (average of last 100 sec per injection cycle) and to determine the percent mitochondrial calcium uptake following successive injections. All methods are as described[25-27].

Mitochondrial swelling assays: Isolated mitochondria were diluted in Isolated Mitochondria Assay Buffer (IMAB; 125 mM KCl, 10 mM NaCl, 20 mM HEPES, 2 mM $MgCl_2$, 2 mM KH_2PO_4, pH 7.2 with KOH). Mitochondria were loaded into 96-well plates (final concentration of 1 µg/µL), supplemented with 10 mM succinate (Sigma-Aldrich, S3674), 10 mM malate (Sigma-Aldrich, 240176) and 10 mM pyruvate (Sigma-Aldrich, P5280). Final volume was 150 µL per well. Absorbance was measured every 5 seconds at 540 nm using a TECAN Infinite M1000 Pro plate reader set at 37°C with plate shaking between measurements. After 2 minutes of baseline measurements, a single Ca^{2+} bolus of 500 µM $CaCl_2$ (7.5 µL of 10 mM $CaCl_2$ stock prepared in IMAB) was administered with measurements recorded every 5 sec for 10 min. All methods are as described[25-27].

Transmission Electron Microscopy (TEM): Left ventricle tissue cut to ~3 mm^3 were fixed in 2% PFA + 2% glutaraldehyde in 0.1 M sodium cacodylate buffer, pH 7.4, and stored at 4°C for 48 h. Tissues were washed 3x for 15 min each in 0.1 M sodium cacodylate buffer, pH 7.4, and then post-fixed in freshly prepared 1.5% potassium ferrocyanide and 1% osmium tetroxide in 0.1 M sodium cacodylate buffer pH 7.4 for 2 h. The samples were washed with water 4x for 15 min each followed by *en bloc* staining overnight with 1% uranyl acetate (aq). Following washing 3x with H_2O for 15 min each, tissues were dehydrated in an ascending acetone series (25% acetone, 50% acetone, 75% acetone, 95% acetone, 100% anhydrous acetone, 100% anhydrous acetone), 15 min each step. Samples were infiltrated with Spurr's resin (25% resin in acetone, 50% resin in acetone, 75% resin in acetone, 100% resin, 100% resin), 1 h each step followed by overnight

incubation in 100% Spurr's resin. The next day, one last exchange in 100% Spurr's resin was performed before samples were placed in aluminum weigh dishes with fresh resin and polymerized at 60ºC overnight. Following polymerization, tissues in proper orientation were excised from the resin with a jeweler's saw and glued onto supports. Muscle tissues were sectioned with a Leica UC7 ultramicrotome, and 60 nm thick sections were collected onto 200 mesh copper grids with a formvar-carbon support film. Grids were post-stained with 2% uranyl acetate in 50% methanol and Reynolds lead citrate. Grids were examined and imaged in a FEI Tecnai 12 120 keV digital TEM, with images acquired at various magnifications (e.g. 1,100x – 21,000x).

Morphometric analysis of TEM images: Analysis of mitochondria, lipid droplets (LD), LD-mitochondria associations, and sarcomere lengths were performed using ImageJ/FIJI (NIH). After calibration for distance, shape descriptors and size measurements were obtained by manually tracing only discernable mitochondria or lipid droplets. Circularity is computed as [4pi × (area/perimeter^2)] and roundness is computed as [4 pi × (surface area)/(pi × major axis^2); values of 1 indicate perfect spheres. Feret Diameter represents the longest distance between any two points within a given mitochondrion[28]. A custom Phyton plugin (MitoCareTools) was adopted for quantification of lipid-mitochondrion associations[29,30]. Areas where the LD was <100nm from the outer mitochondrial membrane (OMM) were determined as a LD-mitochondrion interface. To obtain mean gap distance, the LD membrane was first traced followed by tracing the mitochondrion OMM with values obtained from the plugin.

Protein Immunoblotting: Remaining isolated mitochondria from our calcium and respiratory assays were pelleted and lysed in RIPA buffer supplemented with phosphatase inhibitors (Roche, 4906837001) and protease inhibitors (Sigma, S8830). Samples were kept on ice for 30 min with agitation via vortex every 10 min. Samples were then centrifuged at 13,000 × *g* for 20 min at 4°C. The supernatant was collected, and protein concentration quantified using the Pierce 660nm Protein Assay Reagent (Thermo Fisher Scientific). Equal amounts of protein (5 ug) were run by gel electrophoresis on polyacrylamide Tris-glycine SDS gels. Gels were transferred to PVDF (EMD Milipore, IPFL00010) and membranes were blocked for 1 h in Blocking Buffer (Rockland, MB-070) followed by incubation with primary antibody overnight at 4°C on a rocker. Membranes were then washed in TBS-T 3x for 5 min each and incubated in a fluorescent secondary antibody for 1 h at RT. Membranes were then washed in TBS-T 3x for 5 min each and imaged on a Licor Odyssey system. Antibodies in the study were used at a concentration of 1:1000 and include: VDAC1/3 (Abcam, ab14734), MCU (Cell Signal, 14997), MICU1 (Novus Bio, BP1-86663), MICU2 (Novus Bio, BP2-92063), MCUB (Sigma Aldrich, HPA024771), Total OxPHOS Cocktail (Abcam, ab110413).

RNA sequencing: Left ventricular heart pieces were immediately flash frozen in liquid N_2 following excision and subjected to RNAseq analysis. Total RNA was isolated using a fibrous tissue RNA isolation kit (Qiagen). The TrueSeq stranded mRNA library prep kit was used to enrich polyA mRNAs via poly-T based RNA purification beads which were then amplified using HiSeq rapid SR cluster kit and multiplexed and run using the HiSeq

rapid SBS kit. Reading depth was ~30M reads per sample and single-end 75 bp fragments were generated for bioinformatic analysis. All kits for sequencing were obtained from Illumina and all sequencing was performed on the Illumina HiSeq2500 sequencer. RNA transcripts were aligned to the *Rnor_6.0* assembly using HISAT2 v2.1.0 and quantified using HTSeq v0.11.2. Differential expression analysis was performed between groups using DESeq2 v1.22.2. Genes were considered differentially expressed when they met a fold change ≥2.0 and FDR ≤0.05. Gene ontology (GO) analysis was accomplished using DAVID GO analysis tools. All RNA-sequencing data will be submitted to the GEO repository with the appropriate accession # at time of publication.

Metabolomic analysis: Left ventricular heart pieces were immediately flash frozen in liquid N_2 following excision to most accurately capture the *in vivo* cardiac metabolome. Samples were prepared by Metabolon using their automated MicroLab STAR® system (Hamilton Company, Reno, NV). First, tissue homogenates were made in water at a ratio of 5 µL per mg of tissue. For quality control, several recovery standards were added prior to the first step in the extraction process. To remove protein, dissociate small molecules bound to protein or trapped in the precipitated protein matrix, and to recover chemically diverse metabolites, proteins were then precipitated with methanol (final concentration 80% v/v) under vigorous shaking for 2 min (Glen Mills GenoGrinder 2000) followed by centrifugation. For quality assurance and control, a pooled matrix sample was generated by taking a small volume of each experimental sample to serve as a technical replicate throughout the data set. Extracted water samples served as

process blanks. A cocktail of standards known not to interfere with the measurement of endogenous compounds was spiked into every analyzed sample, allowing instrument performance monitoring and aiding chromatographic alignment.

The extract was divided into fractions for analysis by reverse phase (RP)/UPLC-MS/MS with positive ion mode electrospray ionization (ESI), by RP/UPLC-MS/MS with negative ion mode ESI, and by HILIC/UPLC-MS/MS with negative ion mode ESI. Samples were placed briefly on a TurboVap® (Zymark) to remove the organic solvent. All methods utilized a Waters ACQUITY UPLC and a Thermo Scientific Q-Exactive high resolution/accurate mass spectrometer interfaced with a heated electrospray ionization (HESI-II) source and Orbitrap mass analyzer operated at 35,000 mass resolution. The sample extract was reconstituted in solvents compatible with each MS/MS method. Each reconstitution solvent contained a series of standards at fixed concentrations to ensure injection and chromatographic consistency. One aliquot was analyzed using acidic positive ion conditions, chromatographically optimized for hydrophilic compounds. In this method, the extract was gradient eluted from a C18 column (Waters UPLC BEH C18-2.1×100 mm, 1.7 µm) using water and methanol, containing 0.05% perfluoropentanoic acid (PFPA) and 0.1% formic acid (FA). For more hydrophobic compounds, the extract was gradient eluted from the C18 column using methanol, acetonitrile, water, 0.05% PFPA and 0.01% FA. Aliquots analyzed using basic negative ion optimized conditions were gradient eluted from a separate column using methanol and water, containing 6.5 mM ammonium bicarbonate (pH 8). The last aliquot was analyzed via negative ionization following elution from a HILIC column (Waters UPLC BEH Amide 2.1×150 mm, 1.7 µm) using a gradient consisting of water and acetonitrile

with 10 mM ammonium formate (pH 10.8). The MS analysis alternated between MS and data-dependent MS^n scans using dynamic exclusion. The scan range covered 70–1000 *m/z*.

Raw data were extracted, peak-identified and processed using Metabolon's proprietary hardware and software. Compounds were identified by comparison to library entries of purified, authenticated standards or recurrent unknown entities, with known retention times/indices (RI), mass to charge ratios (*m/z*), and chromatographic signatures (including MS/MS spectral data). Biochemical identifications were based on three criteria: retention index within a narrow RI window of the proposed identification, accurate mass match to the library±10 ppm, and the MS/MS forward and reverse scores between experimental data and authentic standards. Proprietary visualization and interpretation software (Metabolon, Inc., Durham, NC) was used to confirm the consistency of peak identification among the various samples. Library matches for each compound were checked for each sample and corrected, if necessary. Area under the curve was used for peak quantification.

Original scale data (raw area counts) were analyzed using Metaboanalyst 5.0 software (http://www.metaboanalyst.ca/). Metabolites with greater than 50% of the values missing were omitted from the analysis, and missing values were imputed by introducing values with 1/5 of the minimum positive value of each variable. An interquartile range filter was used to identify and remove variables unlikely to be of use when modeling the data. The data were log-transformed and auto-scaled (mean-centered and divided by the standard deviation of each variable). Univariate (e.g., volcano plots) and multivariate (e.g., PCA) analyses were then performed. For multiple

comparison testing, *q* (FDR) values were calculated in R using a method embedded within the Metaboanalyst software, controlling for the false discovery rate. Metabolites were considered significantly different when they met a fold change ≥1.25 and FDR ≤0.05.

Integrated Pathway Network Analyses: Integrated network analyses utilizing both the transcriptomic and metabolomic datasets were performed using Metaboanalyst 5.0 software. Integrated pathway maps were generated using BioRender.

Statistical Analysis: Statistical analysis was performed using GraphPad Prism 9, Metaboanalyst, and the R program. Statistical parameters including the value of n (number of cats), the definition of center, dispersion and precision measures (mean±SEM or SD), and statistical significance is reported in the figures and figure legends. A *P* value of ≤0.05 was considered statistically significant. For the metabolomics and transcriptomics data sets, an FDR value of ≤0.05 was considered statistically significant. For direct comparisons, statistical significance was calculated by unpaired or paired Student *t* test. Details on the statistical methods employed for the metabolomics and RNA-seq data sets can be found within their respective methods sections.

RESULTS

The clinical features of HFpEF are recapitulated in the ZSF1-Obese rat. We investigated whether the ZSF1-Obese rat, which is both hypertensive and obese, phenocopies the clinical characteristics of HFpEF and aimed to identify potential molecular and metabolic mechanisms contributing to HFpEF (**Fig. 1A**); ZSF1-Lean (hypertensive lacking obesity/metabolic syndrome) and WKY rats were included as controls. ZSF1-Obese rats demonstrated a 60% and 40% increase in body weight compared to WKY and ZSF1-Lean controls, respectively (**Fig. 1B**). Both Lean and Obese rats were hypertensive, with elevated systolic (~155 mmHg) and diastolic (~110 mmHg) blood pressures (**Fig. 1C**). Distance run on a treadmill was 83% less in ZSF1-Obese rats, indicating severe exercise intolerance, which was also observed in lean rats (**Fig. 1D**). Echocardiography revealed a significant elevation in the E/e' in ZSF1-Obese rats with preserved ejection fraction (EF%) **(Fig. 1E,F**). Invasive hemodynamics (PV Loop) indicated a 6-fold increase in LVEDP (left ventricular end diastolic pressure; **Fig. 1E**), a hallmark feature distinguishing HFpEF from HFrEF[31]. Left ventricular, atrial, liver, and kidney weights when normalized to tibia length were greatest in ZSF1-Obese rats vs. controls (**Fig. 1G, Supplemental Fig. 1**), indicating tissue hypertrophy and/or edema. Collectively, the ZSF1-Obese rat displays numerous features of clinical HFpEF including obesity, hypertension, exercise intolerance, diastolic dysfunction with preserved ejection fraction, and cardiac hypertrophy.

Lean hypertensive rats demonstrate significant metabolic remodeling with few transcriptional changes. To identify potential molecular and metabolic pathways

contributing to disease development, RNAseq and quantification of the steady-state abundance of metabolites was performed in hearts from all 3 genotypes, initially assessing those changes mediated by hypertension alone by comparing ZSF1-Lean to WKY controls. We observed differential expression of 233 genes in Lean hearts, with 149 increased and 84 decreased in expression (fold change [FC] ≥ 2.0 and FDR ≤ 0.05) (**Fig. 2A**). Gene ontology (GO) analysis of the differentially expressed transcripts surprisingly revealed no significant enrichment of biological or KEGG pathways (**Fig. 2B-E**), suggesting diffuse and non-specific transcriptional remodeling. Metabolomics analysis identified 120 metabolites increased in abundance and 85 decreased in abundance (FC ≥ 1.25 and FDR ≤ 0.05) (**Fig. 2A**). Unlike our transcriptomics dataset, pathway enrichment analysis of the cardiac metabolome revealed significant changes ($p < 0.05$) in nucleotide metabolism, amino acid metabolism, and pathways critical for energy metabolism (e.g., glycolysis, pyruvate, Krebs cycle) (**Fig. 2F**). Collectively, these results suggest that chronic hypertension alone is sufficient to robustly remodel cardiac metabolism while minimally impacting the transcriptome.

ZSF1-Obese HFpEF hearts displays signatures of inflammation, mitochondrial dysfunction, and downregulation of energy metabolism. Based on our physiological phenotyping results, the two-hits of obesity (i.e., metabolic syndrome) and hypertension are required for the robust development of HFpEF. Therefore, while we did examine the transcriptomic and metabolomic differences between ZSF1-Obese and WKY rats (**Supplemental Fig. 2**), we were most interested in identifying potential transcriptional and metabolic alterations revealed with the addition of obesity. A total of 5,691 genes

were differentially expressed (3,123 upregulated and 2,568 downregulated; FC ≥ 2.0 and FDR ≤ 0.05) (**Fig. 3A**). Interestingly, fibrosis and inflammation were the dominant signatures based on GO enrichment analyses, including pathways related to extracellular matrix assembly, immune cell activation, phagocytosis, B cell activation and signaling, immune response, and NF-κB signaling (**Fig. 3B,C**).

GO enrichment analysis of significantly downregulated transcripts revealed suppression of key metabolic and mitochondrial biological processes (**Fig. 3D**). This included the downregulation of ubiquinone biosynthesis, cristae formation, fusion, and protein import into the matrix (**Fig. 3D**). Metabolic pathways that were downregulated in ZSF1-Obese hearts included the Krebs cycle, fatty acid metabolism, and pyruvate metabolism (**Fig. 3E**). In agreement with the transcriptomic analyses, the metabolomic signature was impacted to a greater degree than that observed with hypertension alone (i.e., Lean vs WKY; Fig. 2), with 148 metabolites that were increased and 130 metabolites that decreased in ZSF1-Obese rats as compared to Lean controls (FC ≥ 1.25 and FDR ≤ 0.05) (**Fig. 3A**). Pathway enrichment analysis revealed nucleotide and amino acid metabolism as the most impacted metabolic processes in HFpEF hearts (**Fig. 3F**); although fewer total pathways were significantly impacted, this was due to the underlying metabolic remodeling invoked by hypertension alone. In fact, several metabolites associated with pathways significantly enriched by hypertension alone (e.g., Krebs cycle) were further disrupted in the ZSF1-Obese heart, comparison of the ZSF1-Obese vs WKY in **Supplemental Fig. 2F**, which shows similarly enriched pathways in Lean vs WKY.

Omics integration reveals transcriptional and metabolic coordination of the cardiac energetic deficit in HFpEF. To gain further mechanistic insight into HFpEF development, we next examined transcriptional changes dependent on the two-hits of metabolic syndrome + hypertension versus those independent of hypertension. Changes independent of hypertension included 795 differentially expressed genes (**Supplemental Fig 3A**), with an enrichment in processes related to the cell cycle and proliferation. This transcriptional enrichment could be associated with the meta-inflammation known to occur in HFpEF and which appears evident in the ZSF1-Obese hearts (**Fig. 3B,C** and **Supplemental Fig 3B**). Transcriptional changes dependent on both hypertension and metabolic syndrome revealed 5,544 differentially expressed genes with a significant enrichment in energy metabolism pathways and additional signatures of inflammation (**Supplemental Fig 3C**).

Merger of our omics data sets provides a more comprehensive and integrated interpretation of the remodeling occurring in HFpEF. Using a multi-omics assimilation approach, the differentially expressed transcripts and metabolites significantly altered in abundance were integrated to reveal pathways most impacted that likely contribute to disease progression. The effects of hypertension alone (Lean vs. WKY) indicated glycolysis, purine and pyrimidine metabolism, and nicotinate and nicotinamide metabolism as pathways most impacted (**Fig. 4A**). HFpEF hearts (ZSF1-Obese) had a greater impact on metabolic pathways related to ketone bodies, lipid metabolism, pyruvate metabolism, and the Krebs cycle, which was the most impacted pathway (**Fig. 4B**).

As many of the identified pathways are central to cardiac energy metabolism (i.e., glycolysis, pyruvate metabolism, Krebs cycle), we generated integrated metabolic pathway maps to better illustrate the transcriptional and metabolic changes in these pathways. The hypertensive effects (i.e., ZSF1-Lean vs. WKY) on glycolysis revealed increased expression of *Pfk* (phosphofructokinase) and *Pfkfb1* (6-phosphofructo-2-kinase:fructose-2,6-bisphosphatase), the later which generates fructose-2,6-bisphosphate, a potent allosteric activator of PFK[24]. The downstream glycolytic intermediates 3-phosphoglycerate, 2-phosphoglycerate, phosphoenolpyruvate, and pyruvate were all increased in abundance, potentially suggesting increased glycolytic activity in Lean hearts compared to WKY controls (**Fig. 5A**). This is in stark contrast to the ZSF1-Obese HFpEF heart which showed an overall downregulation of glycolytic enzymes. Obese hearts when compared to Lean had a higher PCr:ATP ratio and lower ATP:ADP ratio than Lean vs WKY, indicating a lower cardiac energy state in HFpEF. These differences were largely driven by a reduction in ATP abundance in the HFpEF heart (**Fig. 5A**). Interestingly, PCr levels were highest in the HFpEF heart, likely in part due to transcriptional downregulation of creatine kinase isoforms (i.e., *Ckm*, *Ckmt2*). Hypertensive and HFpEF hearts demonstrated increased abundance of acyl-carnitines, with greater increases in the two-hit hearts (ZSF1-Obese), suggestive of decreased utilization or increased synthesis (**Fig. 5B, Supplemental Fig. 4**). ZSF1-Obese hearts also showed downregulation of key β-oxidation enzymes and transporters (e.g., *Cact, Cpt1, Cpt2, Acat1*) (**Fig. 5B**). Transcriptional repression of all Krebs cycle enzymes accompanied by increased abundance of the upstream metabolites citrate and isocitrate, suggest an overall decrease in Krebs cycle activity in Obese hearts (**Fig. 5C**).

As glycolysis and β-oxidation are central to cardiac oxidative metabolism, downregulation of their enzymes along with additional pathways capable of input to the Krebs cycle [i.e., branched chain amino acids (BCAAs), ketones, amino acids] also likely contributes to the apparent overall decrease in Krebs cycle activity and the energetic deficit of the HFpEF heart (**Fig 5 and Supplemental Fig. S5**). These integrated analyses reveal a transcriptional and metabolic signature brought upon by obesity in HFpEF, highlighting mitochondrial energy metabolism as a potential distinguishing and important feature.

Disrupted mitochondrial ultrastructure and impaired function are evident early in HFpEF development. Due to the strong mitochondrial signature unique to HFpEF, we looked deeper and examined mitochondrial ultrastructure by transmission electron microscopy. Gross qualitative assessment of electron micrographs revealed mitochondrial cristae disorganization, with less dense cristae observed in the Lean and this progressively worsened in Obese hearts **(Fig 6A)**. Quantitative mitochondrial morphological analyses indicated no difference in mitochondrial number per cardiomyocyte area but a decrease in the total mitochondrial area, indicating smaller mitochondria in Obese hearts (**Fig. 6B**). Damaged or fragmented mitochondria typically assume a smaller and more rounded morphology[32,33], this was evident by a reduction in Feret's diameter and an increase in the circularity index in ZSF1-Obese HFpEF cardiomyocyte mitochondria (**Fig. 6C**). Strikingly, obese hearts displayed a significant increase in lipid droplets (LDs), which localized adjacent to interfibrillar mitochondria (**Fig. 6A**). Quantification of LDs revealed a significant increase in number and size

exclusively in Obese hearts (**Fig. 6D,E**). Because LDs strongly associated with interfibrillar mitochondria, we quantified mitochondria-LD interactions which indicated an increase in the total number of mitochondria-LD contacts as well as the length of mitochondrial and LD membranes in close association with one another (**Fig. 6F**). Lastly, sarcomeric length was increased in ZSF1-Obese cardiomyocytes, likely a consequence of increased preload (i.e., diastolic dysfunction) and LV dilation observed in the HFpEF heart (**Fig. 6G**).

With notable mitochondrial ultrastructural changes, we next examined mitochondrial function via respiratory activity and calcium handling assays. Determination of citrate synthase activity, a gold standard for assessing mitochondrial abundance, was decreased in both Lean and Obese rats (**Fig. 7A**). Both Lean and Obese cardiac mitochondria displayed lower overall respiratory rates as compared with WKY controls (**Fig. 7B,D,F**). In the presence of pyruvate + malate (complex I) or succinate + rotenone (complex II), mitochondria from ZSF1-Lean and -Obese hearts showed a significant reduction in state 3 respiration (**Fig. 7C,E**); fatty acid supported state 3 respiration (palmitoyl-l-carnitine) also trended lower, but did not reach statistical significance (**Fig. 7G**). Complex I respiratory control ratio (RCR) was reduced in the Lean hearts, indicating reduced coupling of oxygen consumption to ATP production, and surprisingly this was improved in the Obese hearts when compared to the reduction in Lean (**Fig. 7C**). No differences were observed for complex II RCR, FAO RCR, or State 4 rates (**Fig. 7E,G and Supplemental Fig. 6A**).

Mitochondrial calcium uptake, is intricately linked to bioenergetics[34] and at high levels induces mitochondrial dysfunction. Indeed, HF is associated with mitochondrial

calcium overload[26,27,34,35]. We isolated mitochondria from ZSF1-Obese hearts and subjected them to repeated 2.5 μM Ca^{2+} boluses. Interestingly, ZSF1-Obese cardiac mitochondria failed to uptake Ca^{2+} as demonstrated by the accumulation of Ca2+ in the bath (i.e., extramitochondrial) (**Fig. 7H,I** and **Supplemental Fig. 6B**). This is suggestive of mitochondria that are either already calcium-overloaded or that have downregulated mitochondrial calcium uniporter activity. Mitochondrial swelling, an indicator of susceptibility to mitochondrial permeability transition, was increased in Lean hearts while swelling of ZSF1-Obese HFpEF mitochondria occurred faster and to a greater extent than both WKY and Lean mitochondria (**Fig. 7J-M and Supplemental Fig. 6C**). Protein expression via immunoblotting of proteins involved in mitochondrial Ca^{2+} handling revealed a significant increase in both the 30 kDa and 40 kDa MCU isoforms and in the MCU gatekeeper, MICU1, exclusively in ZSF1-Obese HFpEF cardiac mitochondria when normalized to a mitochondrial loading control, ATP synthase (i.e., complex V) (**Fig. 7N,O and Supplemental Fig. 7**). VDAC1, which is also involved in mitochondrial calcium homeostasis[34], was significantly decreased in ZSF1-Obese mitochondria (**Fig. 7N**). Collectively, our results indicate significant remodeling of the mitochondrial ultrastructure, accumulation of cardiomyocyte lipid droplets, dysfunctional respiratory capacity, and dysregulated calcium handling all of which underlie and likely contribute to the gross metabolic dysregulation and subsequent cardiac dysfunction observed in the HFpEF heart.

DISCUSSION

In the present study, we characterized and identified the underlying molecular changes associated with the HFpEF phenotype in a robust preclinical rat model. Key findings include:

- Metabolic syndrome/obesity is a principal driver of HFpEF
- Transcriptional and metabolic remodeling in HFpEF is characterized by the upregulation of inflammation and downregulation of energy metabolism
- Mitochondrial ultrastructural and functional remodeling underlie the HFpEF phenotype and likely is an early contributor to cardiac dysfunction.
- The HFpEF heart displays significant intramyocardial lipid accumulation (huge increase in lipid droplet size, number, and association with mitochondria).

Impact of the additive hit of metabolic syndrome and obesity

The ZSF1-Obese rat model recapitulates the multifactorial clinical features that distinguish HFpEF. Importantly, our study validates the notion that “two-hits”, hypertension and metabolic syndrome/obesity are necessary for the development of HFpEF, similar to the L-name + HFD murine model[11] and in agreement with human HFpEF populations which are typically obese with vascular dyfunction[36,37]. A strength of our study is the inclusion of the WKY non-hypertensive control as this allowed us to examine transcription, metabolic, and functional changes that are dependent and independent of these “two-hits”. While hypertension alone resulted in cardiac metabolic remodeling, the addition of metabolic syndrome resulted in more drastic metabolic remodeling which was associated with an energetic deficit and mitochondrial abnormalities, both in ultrastructure and function. Similarly, only 152 transcription

585 changes were exclusively dependent upon hypertension, whereas 795 transcripts
586 independent of hypertension and 5,544 transcript changes were dependent on both
587 metabolic syndrome and hypertension. While other models of HFpEF have been
588 proposed, namely models of Western diet feeding[9], angiotensin II/phenylephrine
589 (ANGII/PE) infusion[8], and senescence-accelerated aging (i.e., SAMP/SAMPR mice)[10,12],
590 and while pathology associated with these models may be multifactorial, these models
591 do not contain two independent hits. Furthermore, long-term Western diet feeding
592 progresses to HFrEF, which rarely occurs in humans[38,39], and ANGII/PE and
593 SAMP/SAMPR models lack metabolic syndrome and/or hypertension. While these
594 models are likely suitable for the study of diastolic dysfunction, this is distinct from the
595 multifaceted, multi-organ nature of HFpEF. Thus, the ZSF1-obese rat model serves as
596 an excellent preclinical model to study cardiometabolic HFpEF.

597 Identifying therapeutic targets for HFpEF has proven difficult due to the
598 combinatorial etiologies that contribute to the syndrome. Recently, SGLT2 inhibitors
599 (SGLT2i), which act to block glucose reabsorption in the kidney, have proven efficacious
600 and safe in reducing cardiovascular events in animal models[40,41] and in HFpEF
601 trials[42,43]. SGLT2i have a minimal impact on hypertension yet result in profound weight
602 loss and normalization towards glucose homeostasis[40,44,45]. These results are directly in
603 line with our findings and overall conclusion that the primary driver of HFpEF is the
604 metabolic syndrome component, which is further exacerbated in the Obese- vs Lean-
605 ZSF1 rats. Adjunctive therapy of SGLT2i + a hydrogen sulfide donor (H_2S, a well-
606 studied cardioprotective agent) in our ZSF1-Obese HFpEF model was shown to be
607 efficaciously superior to either treatment alone[19]. This is interesting as H2S has been

shown to modulate metabolism[23] and preserve mitochondrial integrity[46]. While we observed numerous transcriptional changes independent of hypertension, most of the transcriptional remodeling was dependent on both hits, thus, treatments aimed at targeting metabolic syndrome alone will likely be insufficient for long-term efficacy.

Our study provides a roadmap for the discovery of novel mechanisms driving HFpEF progression and provides a data set which can be correlated to the remodeling observed in human HFpEF[47]. Targeting of HDAC6 in a HFpEF mouse model was recently shown to be as efficacious as SGLT2i[41]. This is of note as the mechanisms of SGLT2i cardioprotection remains unclear as mice with global loss of SGLT2 are protected from HF with SGLT2 blockade[48,49], indicating SGLT2 inhibitors likely have an off-target mechanism of action.

Remodeling of Energy Metabolism

An important observation from our metabolomics dataset is a drastic change in the energy state of the ZSF1-Obese heart. HFpEF hearts displayed a greater PCr:ATP ratio (1.85 vs 0.884) and lower ATP:ADP ratio (0.37 vs 4.87) as compared to hypertension alone. This was driven by a significant reduction in ATP in the HFpEF heart. This may, in part, be associated with an inability to liberate PCr stores, as all creatine kinase isoforms were reduced in ZSF1-Obese rats. This indicates that the HFpEF heart is energy starved, as compared to the ZSF1-Lean control (hypertension alone). The ZSF1-Obese heart also displayed gross metabolic remodeling of pathways associated with energy metabolism, discussed hereafter.

Glycolysis – We observed an increase in the expression of *Pfkl* and of *Pfkfb1*, activators of aerobic glycolysis, and downstream metabolites of glycolysis (i.e., 3-PG, 2-PG, PEP, and pyruvate) were also found to be increased, suggesting increased glycolysis in the hypertensive heart. In contrast, nearly all glycolytic enzymes were decreased in abundance in the Obese HFpEF heart. These results are in agreement with results from the Kass Lab which also found a reduction in protein expression of these same glycolytic enzymes in human HFpEF endomyocardial biopsies; however, they only detected decreased abundance of the upstream glycolytic metabolites G6P and F-1,6-BP while we observed a decrease in the downstream metabolite PEP[50]. Glucose oxidation is also likely decreased as we and others have shown changes in the abundance of pyruvate, PDH, MPC1, and PDK4[50,51], with direct measurements of reduced glucose oxidation performed in the working heart[52]. Both in the ZSF1-Obese and human HFpEF heart, changes in the pentose phosphate pathway (i.e., purine and pyrimidine metabolism) were identified, indicating disruptions to ancillary biosynthetic pathways; these ancillary pathways are known to contribute to cardiac remodeling[53,54], highlighting that their role in HFpEF is an area worthy of investigation. Collectively, these studies suggest a significant downregulation of glycolytic metabolism and changes in ancillary pathways in the HFpEF heart.

Fatty Acids – Fatty acids contribute the largest percentage to cardiac energy production, thus loss of oxidative capacity in the failing heart would be detrimental to energy metabolism and cardiac function. Our results indicate a significant impairment in fatty acid oxidation (FAO), with associated FA metabolic processes among the most

654 downregulated in the HFpEF heart, including key enzymes in transport and processing
655 (e.g., *Acs*, *Cpt1*, *Cact*, *Acad*, *Acat1*). Dysregulation of genes involved in fatty acid and
656 oxidative metabolism seems a conserved signature, as similar findings to ours have
657 been shown in other murine models[41,55] and human HFpEF populations[51]; however,
658 some studies have reported an increase in FAO transcripts[56]. While there is a
659 discrepancy in gene expression among different studies, a proteomic study of HFpEF
660 samples, from the same group that reported an increase in FAO and OXPHOS
661 transcripts, found an overall decrease in protein abundance[57], a reminder that transcript
662 and protein abundance often do not correlate in pathology.

663 In agreement with a decrease in FAO, our results indicate reduced abundance of
664 short chain acyl-carnitines and increased medium and long-chain acylcarnitines,
665 potentially suggesting inefficient oxidation. Medium and long-chain acylcarnitines were
666 decreased in human HFpEF and the expression of FAO genes were also decreased[51];
667 whether this discrepancy in findings is simply due to sampling of the right ventricle
668 versus the left ventricle remains to be determined. Nonetheless, Krebs cycle
669 intermediates are lower in human HFpEF[51] and we demonstrate reduced utilization of
670 fatty acids by mitochondria isolated from HFpEF hearts. While these collective results
671 suggest impairments in fatty acid utilization, palmitate oxidation measured in the
672 isolated working heart was increased in the mouse L-name + HFD mouse model[52];
673 thus, more work is needed to define how HFpEF remodels cardiac fatty acid
674 metabolism.
675

Ketones, BCAAs, and Amino Acids – The potential for alternative fuel sources to contribute to cardiac energetics has become more appreciated. Our integrated network analysis approach identified the synthesis and degradation of ketone bodies as highly impacted in HFpEF. We observed an increase in 3-hydroxybutyrate and a corresponding decrease in key ketone catabolic enzymes (i.e., *Bdh1*, *Oxtc1*, *Acat1*), suggestive of reduced utilization. In a murine model of HFpEF, BDH1 protein abundance is reduced with a corresponding trend of decreased oxidation rates[52]. In HFrEF, myocardial uptake, oxidation, and expression of BDH1 increases 2- to 3-fold[58-60], which is greater than predicted rates in HFpEF[59]. This divergence in ketone body oxidation between HFrEF and HFpEF may provide insight into differential substrate/fuel treatment strategies. For example, while increasing circulating ketones through the diet appears to provide beneficial effects in HFrEF[61], whether this would be beneficial in HFpEF has not been explored. Another potential target could be HMGCS, which we found upregulated in the ZSF1-Obese HFpEF heart and is generally known to be involved in ketone synthesis; thus, whether impaired ketone oxidation is due to competing synthesis mediated by HMGCS presents an interesting inquiry.

The branched chain amino acids (BCAAs) leucine, valine, and isoleucine have been proposed as an alternative fuel source for the heart and suppression of BCAA oxidation has been implicated in heart failure[62,63]. While we observed a global suppression of BCAA oxidation genes, the downregulation of the nodal BCAA catabolic enzyme, branched-chain α-keto acid dehydrogenase complex (*Bckdh*), agrees with data in human HFpEF[51]. Previous reports suggest BCAAs accumulate in the human HFpEF heart, suggesting decreased oxidation[64]. However, contributions of BCAAs

699 to energy production are likely minimal[59,62,65,66] and the activation of cardiac BCAA
700 oxidation does not provide energetic or functional benefit in models of HFrEF[67].
701 Thus, while BCAA oxidation seems downregulated, targeting this pathway in HFpEF
702 may not prove effective.

703 Our integrated pathway maps identified the downregulation of numerous other
704 amino acid pathways at the level of transcription and/or metabolite abundance. The
705 observed changes in global amino acid metabolism could be related to the increased
706 proteolysis that occurs in the failing heart[59]. Many of these amino acids and represented
707 pathways have yet to be explored, providing experimental opportunities to generate new
708 hypotheses. For example, we observed a reduction in arginine metabolism, which when
709 given as an oral supplement to HFrEF patients proved beneficial[68]; whether similar
710 benefits could be obtained in HFpEF patients is worth exploring.

711

712 **Impact on Mitochondrial and Lipid Droplet Structure and Function**

713 *Ultrastructural changes* – Mitochondrial dysfunction is a hallmark of HF[69-71] and our
714 transcriptomic and metabolic signatures implicates the derangement of several
715 mitochondrial processes in the ZSF1-Obese heart. Downregulation of biological
716 processes related to cristae formation and mitochondrial fusion were confirmed by
717 ultrastructural remodeling characterized by the disruption and near disappearance of
718 cristae and overall smaller and more rounded mitochondria, indicating that the fission-
719 fusion balance is perturbed. Alterations in mitochondrial shape and cristae density can
720 greatly impact the localization, structure and function of the OXPHOS system, impairing
721 cellular and mitochondrial metabolism[32,33,72]. While we observed no change in total

mitochondrial number, mitochondrial area was significantly reduced in HFpEF, likely because the smaller size of individual mitochondrions. Interesting, mice treated with the SGLT2i empagliflozin demonstrated an increase in mitochondrial area per cardiomyocyte area[40]. Recently, TEM of human HFpEF cardiomyocytes revealed no change in mitochondrial area but significant cristae derangement which was most observable in patients presenting with obesity[57].

There exists a high correlation between myocardial adiposity and diastolic dysfunction[73,74]. Cardiac MRI of HFpEF, HFrEF, and non-failing patients revealed significant intramyocardial fat only in HFpEF[75]. We observed the accumulation of LDs in HFpEF hearts which was also recently seen in HFpEF patients via TEM imaging[57]. LDs act as an energy storage depot and are involved in transferring stored FAs to mitochondria for energy production. However, transcriptional downregulation of fatty acid oxidation machinery and the structural remodeling likely limit utilization, thus promoting storage and LD accumulation. While we observed greater mito-LD interactions in HFpEF, the interpretation of this result is confounded by the fact that few, if any LDs were observed in control hearts. To overcome this limitation, we examined the expression of known proteins that act as tethers to support mitochondria and lipid droplets approximation. Perilipin 5 (PLIN5), a LD protein reported to tether them to mitochondria[76,77], was downregulated 3-fold in our HFpEF hearts. Loss of PLIN5 decreases mito-LD interactions and oxidative metabolism, whereas overexpression increases these interactions[78]. Similarly, we noted a downregulation of *Miga2*, another mito-LD tether involved in lipid metabolism and mitochondrial fusion[79,80]. Whether

744 disruption of these tethers could play a role in HFpEF is unknown, but it's striking that
745 these LD proteins were downregulated in the context of massive LD biogenesis.
746
747 *Mitochondrial Dysfunction* – Mitochondrial respiratory capacity was significantly
748 impaired in both the pre-HFpEF (hypertensive) and HFpEF (hypertension + metabolic
749 syndrome) heart, suggesting that while mitochondrial dysfunction is a key feature of HF,
750 it is not necessarily unique to HFpEF. What is unique in the HFpEF heart is impaired
751 mitochondrial calcium handling. Mitochondrial protein expression of MCU and MICU1,
752 components of the mitochondrial calcium uniporter, were increased exclusively in the
753 HFpEF heart. This could be a compensatory change to increase calcium-dependent
754 activation of mitochondrial dehydrogensases to increase Krebs cycle flux and
755 mitochondrial energetics. However, as previously reported by our group and others,
756 while initially compensatory these expression changes in uniporter components turns
757 maladaptive with chronic stress (refs). In a mouse model of HFpEF, SGLT2i treatment
758 improved HFpEF-mediated Ca^{2+} reuptake by the sarcoplasmic reticulum and rescued
759 mitochondrial respiratory function[40]; however, whether improved reuptake was a
760 consequence of improving mitochondrial Ca^{2+} buffering, improved energetics, and/or
761 enhancing SERCA activity was not tested. Similarly, treating HF with a pan HDAC
762 inhibitor (SAHA) decreased acetylation of proteins involved in oxidative metabolism,
763 improving mitochondrial oxidative phosphorylation[81]. Whether HDAC inhibition plays a
764 similarly protective role in HFpEF remains to be investigated.
765

Study Limitations. There are several limitations to our study. Our results do not test a specific mechanism or hypothesis but provide an integrated systems biology approach to allow for the discovery of potentially important pathways and mechanisms contributing to HFpEF. The current study also exclusively utilized male rats, partly due to the high-cost of acquiring a sufficient number of female rats to maintain power in our dual-control study. However, a recent study that exclusively utilized ZSF1 female rats reported similar findings related to the mitochondria[40], suggesting conserved mechanisms of action between sexes. Adjusting for sex in a human HFpEF RNAseq study, importantly, did not affect pathway enrichment[56]. Nonetheless, as the prevalence of HFpEF is slightly greater in females than males, we understand and acknowledge the importance of potential for sex differences in molecular pathways. Current work in our labs is exploring whether similar functional, metabolic, transcriptional, and mitochondrial remodeling is found in female HFpEF or whether sex distinguishes between remodeling pathways and targets. Also, aging is a critical risk factor for HFpEF and is not accounted for in our study. As we have shown in a large animal model of diastolic dysfunction, aging alone significantly alters the cardiac transcriptome and metabolome[7], making it difficult to tease out pathway changes due to disease progression, aging, or both. Lastly, it is evident that metabolic syndrome and obesity are primary drivers of HFpEF development, thus understanding the systemic changes at peripheral tissues is critical to complete our understanding of HFpEF pathophysiology. In a large-animal model that recapitulates several clinical features of HFpEF and diastolic dysfunction, we found skeletal muscle to have distinct transcriptional and metabolic signatures that were accompanied by mitochondrial dysfunction[7], and similar findings have been noted in

human HFpEF skeletal muscle[82]. Similar approaches have also been performed to identify potential candidates for interorgan crosstalk between the liver and heart in HFpEF[83]. Investigating peripheral tissues and potential interorgan communication likely will yield novel and meaningful insights to understand HFpEF development and progression.

CONCLUSIONS

In summary, the results presented here demonstrate the power of applying integrated omics technologies to lead to the design of functional experiments to test specific hypotheses and discover novel therapeutic targets. The ZSF1-Obese rat model recapitulates the clinical characteristics of human HFpEF and shares many of the same transcriptional, metabolic, and mitochondrial remodeling as seen in patients. Our findings provide a wealth of data that are likely to reveal novel metabolic pathways and molecular targets which will hopefully allow for the discovery of new therapeutics to treat HFpEF.

Acknowledgements:

AAG, DJL, and JWE were involved in conception and design. AAG, KL, RBG, YT, CCF, JD, ZL, HX, MPL, NL, MC, TS, TTG, DJL, and JWE were involved in data collection, analysis, and interpretation. AAG, DJL, and JWE were involved in drafting the manuscript and revision of the manuscript. All authors were involved in final approval of the manuscript submitted. We would also like to thank Shannon Modla and Jean Ross in the University of Delaware Bio-Imaging Center for assistance in tissue processing for TEM and Gyorgy Csordas and Timothy Schneider at Thomas Jefferson University Mito Care Center for assisting in TEM image acquisition.

Funding Sources:

This work was supported in part by grants from the NIH (F32HL145914) and AHA (Career Development Award; 937591) to AAG, AHA postdoctoral fellowship (20POST35200075) to ZL, JED is the recipient of a training fellowship from the NIH National CCTS awarded to the University of Alabama at Birmingham (TL1TR00316), NIH (F30HL152564) to MPL, National Institute of Alcohol Abuse and Alcoholism (AA029984) to TES, NIH (HL159428) to TTG, NIH (HL146098, HL146514, HL151398) to DJL, and NIH (R01NS121379, P01HL147841, 2P01HL134608, T32HL091804) and AHA (20EIA35320226) to JWE.

REFERENCES

1. Borlaug BA, Sharma K, Shah SJ, Ho JE. Heart Failure With Preserved Ejection Fraction: JACC Scientific Statement. *J Am Coll Cardiol*. 2023;81:1810-1834. doi: 10.1016/j.jacc.2023.01.049
2. Tsao CW, Aday AW, Almarzooq ZI, Anderson CAM, Arora P, Avery CL, Baker-Smith CM, Beaton AZ, Boehme AK, Buxton AE, et al. Heart Disease and Stroke Statistics-2023 Update: A Report From the American Heart Association. *Circulation*. 2023;147:e93-e621. doi: 10.1161/CIR.0000000000001123
3. Jeffries A, Chan WPA. Heart Failure with Preserved Ejection Fraction: Advances in Management Medicine Today. *Medicine Today*. 2023;24:21-27.
4. Sayed A, Abramov D, Fonarow GC, Mamas MA, Kobo O, Butler J, Fudim M. Reversals in the Decline of Heart Failure Mortality in the US, 1999 to 2021. *JAMA Cardiol*. 2024;9:585-589. doi: 10.1001/jamacardio.2024.0615
5. Hamo CE, DeJong C, Hartshorne-Evans N, Lund LH, Shah SJ, Solomon S, Lam CSP. Heart failure with preserved ejection fraction. *Nat Rev Dis Primers*. 2024;10:55. doi: 10.1038/s41572-024-00540-y
6. Shah SJ, Borlaug BA, Kitzman DW, McCulloch AD, Blaxall BC, Agarwal R, Chirinos JA, Collins S, Deo RC, Gladwin MT, et al. Research Priorities for Heart Failure With Preserved Ejection Fraction: National Heart, Lung, and Blood Institute Working Group Summary. *Circulation*. 2020;141:1001-1026. doi: 10.1161/CIRCULATIONAHA.119.041886
7. Gibb AA, Murray EK, Eaton DM, Huynh AT, Tomar D, Garbincius JF, Kolmetzky DW, Berretta RM, Wallner M, Houser SR, et al. Molecular Signature of HFpEF: Systems Biology in a Cardiac-Centric Large Animal Model. *JACC Basic Transl Sci*. 2021;6:650-672. doi: 10.1016/j.jacbts.2021.07.004
8. Matsiukevich D, Kovacs A, Li T, Kokkonen-Simon K, Matkovich SJ, Oladipupo SS, Ornitz DM. Characterization of a robust mouse model of heart failure with preserved ejection fraction. *Am J Physiol Heart Circ Physiol*. 2023;325:H203-H231. doi: 10.1152/ajpheart.00038.2023
9. Maurya SK, Carley AN, Maurya CK, Lewandowski ED. Western Diet Causes Heart Failure With Reduced Ejection Fraction and Metabolic Shifts After Diastolic Dysfunction and Novel Cardiac Lipid Derangements. *JACC Basic Transl Sci*. 2023;8:422-435. doi: 10.1016/j.jacbts.2022.10.009
10. Reed AL, Tanaka A, Sorescu D, Liu H, Jeong EM, Sturdy M, Walp ER, Dudley SC, Jr., Sutliff RL. Diastolic dysfunction is associated with cardiac fibrosis in the senescence-accelerated mouse. *Am J Physiol Heart Circ Physiol*. 2011;301:H824-831. doi: 10.1152/ajpheart.00407.2010
11. Schiattarella GG, Altamirano F, Tong D, French KM, Villalobos E, Kim SY, Luo X, Jiang N, May HI, Wang ZV, et al. Nitrosative stress drives heart failure with preserved ejection fraction. *Nature*. 2019;568:351-356. doi: 10.1038/s41586-019-1100-z
12. Takeda T, Matsushita T, Kurozumi M, Takemura K, Higuchi K, Hosokawa M. Pathobiology of the senescence-accelerated mouse (SAM). *Exp Gerontol*. 1997;32:117-127. doi: 10.1016/s0531-5565(96)00068-x

13. van Dijk CG, Oosterhuis NR, Xu YJ, Brandt M, Paulus WJ, van Heerebeek L, Duncker DJ, Verhaar MC, Fontoura D, Lourenco AP, et al. Distinct Endothelial Cell Responses in the Heart and Kidney Microvasculature Characterize the Progression of Heart Failure With Preserved Ejection Fraction in the Obese ZSF1 Rat With Cardiorenal Metabolic Syndrome. *Circ Heart Fail*. 2016;9:e002760. doi: 10.1161/CIRCHEARTFAILURE.115.002760
14. Hamdani N, Franssen C, Lourenco A, Falcao-Pires I, Fontoura D, Leite S, Plettig L, Lopez B, Ottenheijm CA, Becher PM, et al. Myocardial titin hypophosphorylation importantly contributes to heart failure with preserved ejection fraction in a rat metabolic risk model. *Circ Heart Fail*. 2013;6:1239-1249. doi: 10.1161/CIRCHEARTFAILURE.113.000539
15. Tofovic SP, Jackson EK. Rat models of the metabolic syndrome. *Methods Mol Med*. 2003;86:29-46. doi: 10.1385/1-59259-392-5:29
16. Leite S, Oliveira-Pinto J, Tavares-Silva M, Abdellatif M, Fontoura D, Falcao-Pires I, Leite-Moreira AF, Lourenco AP. Echocardiography and invasive hemodynamics during stress testing for diagnosis of heart failure with preserved ejection fraction: an experimental study. *Am J Physiol Heart Circ Physiol*. 2015;308:H1556-1563. doi: 10.1152/ajpheart.00076.2015
17. Schauer A, Draskowski R, Jannasch A, Kirchhoff V, Goto K, Mannel A, Barthel P, Augstein A, Winzer E, Tugtekin M, et al. ZSF1 rat as animal model for HFpEF: Development of reduced diastolic function and skeletal muscle dysfunction. *ESC Heart Fail*. 2020;7:2123-2134. doi: 10.1002/ehf2.12915
18. Doiron JE, Li Z, Yu X, LaPenna KB, Quiriarte H, Allerton TD, Koul K, Malek A, Shah SJ, Sharp TE, et al. Early Renal Denervation Attenuates Cardiac Dysfunction in Heart Failure With Preserved Ejection Fraction. *J Am Heart Assoc*. 2024;13:e032646. doi: 10.1161/JAHA.123.032646
19. Doiron JE, Xia H, Yu X, Nevins AR, LaPenna KB, Sharp TE, 3rd, Goodchild TT, Allerton TD, Elgazzaz M, Lazartigues E, et al. Adjunctive therapy with an oral H(2)S donor provides additional therapeutic benefit beyond SGLT2 inhibition in cardiometabolic heart failure with preserved ejection fraction. *Br J Pharmacol*. 2024;181:4294-4310. doi: 10.1111/bph.16493
20. Nguyen ITN, Brandt MM, van de Wouw J, van Drie RWA, Wesseling M, Cramer MJ, de Jager SCA, Merkus D, Duncker DJ, Cheng C, et al. Both male and female obese ZSF1 rats develop cardiac dysfunction in obesity-induced heart failure with preserved ejection fraction. *PLoS One*. 2020;15:e0232399. doi: 10.1371/journal.pone.0232399
21. Tong D, Schiattarella GG, Jiang N, May HI, Lavandero S, Gillette TG, Hill JA. Female Sex Is Protective in a Preclinical Model of Heart Failure With Preserved Ejection Fraction. *Circulation*. 2019;140:1769-1771. doi: 10.1161/CIRCULATIONAHA.119.042267
22. Li Z, Xia H, Sharp TE, 3rd, LaPenna KB, Katsouda A, Elrod JW, Pfeilschifter J, Beck KF, Xu S, Xian M, et al. Hydrogen Sulfide Modulates Endothelial-Mesenchymal Transition in Heart Failure. *Circ Res*. 2023;132:154-166. doi: 10.1161/CIRCRESAHA.122.321326
23. Li Z, Xia H, Sharp TE, 3rd, LaPenna KB, Elrod JW, Casin KM, Liu K, Calvert JW, Chau VQ, Salloum FN, et al. Mitochondrial H(2)S Regulates BCAA Catabolism in

Heart Failure. *Circ Res*. 2022;131:222-235. doi: 10.1161/CIRCRESAHA.121.319817

24. Gibb AA, Epstein PN, Uchida S, Zheng Y, McNally LA, Obal D, Katragadda K, Trainor P, Conklin DJ, Brittian KR, et al. Exercise-Induced Changes in Glucose Metabolism Promote Physiological Cardiac Growth. *Circulation*. 2017;136:2144-2157. doi: 10.1161/CIRCULATIONAHA.117.028274
25. Lambert JP, Luongo TS, Tomar D, Jadiya P, Gao E, Zhang X, Lucchese AM, Kolmetzky DW, Shah NS, Elrod JW. MCUB Regulates the Molecular Composition of the Mitochondrial Calcium Uniporter Channel to Limit Mitochondrial Calcium Overload During Stress. *Circulation*. 2019;140:1720-1733. doi: 10.1161/CIRCULATIONAHA.118.037968
26. Luongo TS, Lambert JP, Gross P, Nwokedi M, Lombardi AA, Shanmughapriya S, Carpenter AC, Kolmetzky D, Gao E, van Berlo JH, et al. The mitochondrial Na+/Ca2+ exchanger is essential for Ca2+ homeostasis and viability. *Nature*. 2017;545:93-97. doi: 10.1038/nature22082 http://www.nature.com/nature/journal/v545/n7652/abs/nature22082.html#supplementary-information
27. Luongo Timothy S, Lambert Jonathan P, Yuan A, Zhang X, Gross P, Song J, Shanmughapriya S, Gao E, Jain M, Houser Steven R, et al. The Mitochondrial Calcium Uniporter Matches Energetic Supply with Cardiac Workload during Stress and Modulates Permeability Transition. *Cell Reports*. 2015;12:23-34. doi: 10.1016/j.celrep.2015.06.017
28. Picard M, White K, Turnbull DM. Mitochondrial morphology, topology, and membrane interactions in skeletal muscle: a quantitative three-dimensional electron microscopy study. *J Appl Physiol (1985)*. 2013;114:161-171. doi: 10.1152/japplphysiol.01096.2012
29. Chen Y, Csordas G, Jowdy C, Schneider TG, Csordas N, Wang W, Liu Y, Kohlhaas M, Meiser M, Bergem S, et al. Mitofusin 2-containing mitochondrial-reticular microdomains direct rapid cardiomyocyte bioenergetic responses via interorganelle Ca(2+) crosstalk. *Circ Res*. 2012;111:863-875. doi: 10.1161/CIRCRESAHA.112.266585
30. Nichtova Z, Fernandez-Sanz C, De La Fuente S, Yuan Y, Hurst S, Lanvermann S, Tsai HY, Weaver D, Baggett A, Thompson C, et al. Enhanced Mitochondria-SR Tethering Triggers Adaptive Cardiac Muscle Remodeling. *Circ Res*. 2023;132:e171-e187. doi: 10.1161/CIRCRESAHA.122.321833
31. Gori M, Iacovoni A, Senni M. Haemodynamics of Heart Failure With Preserved Ejection Fraction: A Clinical Perspective. *Card Fail Rev*. 2016;2:102-105. doi: 10.15420/cfr.2016:17:2
32. MacMullen C, Davis RL. High-Throughput Phenotypic Assay for Compounds That Influence Mitochondrial Health Using iPSC-Derived Human Neurons. *SLAS Discov*. 2021;26:811-822. doi: 10.1177/24725552211000671
33. Varkuti BH, Kepiro M, Liu Z, Vick K, Avchalumov Y, Pacifico R, MacMullen CM, Kamenecka TM, Puthanveettil SV, Davis RL. Neuron-based high-content assay and screen for CNS active mitotherapeutics. *Sci Adv*. 2020;6:eaaw8702. doi: 10.1126/sciadv.aaw8702

34. Garbincius JF, Elrod JW. Mitochondrial calcium exchange in physiology and disease. *Physiol Rev*. 2022;102:893-992. doi: 10.1152/physrev.00041.2020
35. Garbincius JF, Luongo TS, Jadiya P, Hildebrand AN, Kolmetzky DW, Mangold AS, Roy R, Ibetti J, Nwokedi M, Koch WJ, et al. Enhanced NCLX-dependent mitochondrial Ca(2+) efflux attenuates pathological remodeling in heart failure. *J Mol Cell Cardiol*. 2022;167:52-66. doi: 10.1016/j.yjmcc.2022.03.001
36. Haass M, Kitzman DW, Anand IS, Miller A, Zile MR, Massie BM, Carson PE. Body mass index and adverse cardiovascular outcomes in heart failure patients with preserved ejection fraction: results from the Irbesartan in Heart Failure with Preserved Ejection Fraction (I-PRESERVE) trial. *Circ Heart Fail*. 2011;4:324-331. doi: 10.1161/CIRCHEARTFAILURE.110.959890
37. Rao VN, Zhao D, Allison MA, Guallar E, Sharma K, Criqui MH, Cushman M, Blumenthal RS, Michos ED. Adiposity and Incident Heart Failure and its Subtypes: MESA (Multi-Ethnic Study of Atherosclerosis). *JACC Heart Fail*. 2018;6:999-1007. doi: 10.1016/j.jchf.2018.07.009
38. Borlaug BA, Redfield MM. Diastolic and systolic heart failure are distinct phenotypes within the heart failure spectrum. *Circulation*. 2011;123:2006-2013; discussion 2014. doi: 10.1161/CIRCULATIONAHA.110.954388
39. Rame JE, Ramilo M, Spencer N, Blewett C, Mehta SK, Dries DL, Drazner MH. Development of a depressed left ventricular ejection fraction in patients with left ventricular hypertrophy and a normal ejection fraction. *Am J Cardiol*. 2004;93:234-237. doi: 10.1016/j.amjcard.2003.09.050
40. Schauer A, Adams V, Kammerer S, Langner E, Augstein A, Barthel P, Mannel A, Fabig G, Alves PKN, Gunscht M, et al. Empagliflozin Improves Diastolic Function in HFpEF by Restabilizing the Mitochondrial Respiratory Chain. *Circ Heart Fail*. 2024;17:e011107. doi: 10.1161/CIRCHEARTFAILURE.123.011107
41. Ranjbarvaziri S, Zeng A, Wu I, Greer-Short A, Farshidfar F, Budan A, Xu E, Shenwai R, Kozubov M, Li C, et al. Targeting HDAC6 to treat heart failure with preserved ejection fraction in mice. *Nat Commun*. 2024;15:1352. doi: 10.1038/s41467-024-45440-7
42. Solomon SD, McMurray JJV, Claggett B, de Boer RA, DeMets D, Hernandez AF, Inzucchi SE, Kosiborod MN, Lam CSP, Martinez F, et al. Dapagliflozin in Heart Failure with Mildly Reduced or Preserved Ejection Fraction. *New England Journal of Medicine*. 2022. doi: 10.1056/NEJMoa2206286
43. Anker SD, Butler J, Filippatos G, Ferreira JP, Bocchi E, Bohm M, Brunner-La Rocca HP, Choi DJ, Chopra V, Chuquiure-Valenzuela E, et al. Empagliflozin in Heart Failure with a Preserved Ejection Fraction. *N Engl J Med*. 2021;385:1451-1461. doi: 10.1056/NEJMoa2107038
44. Ye N, Jardine MJ, Oshima M, Hockham C, Heerspink HJL, Agarwal R, Bakris G, Schutte AE, Arnott C, Chang TI, et al. Blood Pressure Effects of Canagliflozin and Clinical Outcomes in Type 2 Diabetes and Chronic Kidney Disease: Insights From the CREDENCE Trial. *Circulation*. 2021;143:1735-1749. doi: 10.1161/CIRCULATIONAHA.120.048740
45. Habibi J, Aroor AR, Sowers JR, Jia G, Hayden MR, Garro M, Barron B, Mayoux E, Rector RS, Whaley-Connell A, et al. Sodium glucose transporter 2 (SGLT2) inhibition with empagliflozin improves cardiac diastolic function in a female rodent

model of diabetes. *Cardiovasc Diabetol*. 2017;16:9. doi: 10.1186/s12933-016-0489-z

46. Elrod JW, Calvert JW, Morrison J, Doeller JE, Kraus DW, Tao L, Jiao X, Scalia R, Kiss L, Szabo C, et al. Hydrogen sulfide attenuates myocardial ischemia-reperfusion injury by preservation of mitochondrial function. *Proc Natl Acad Sci U S A*. 2007;104:15560-15565. doi: 10.1073/pnas.0705891104
47. Bornstein MR, Tian R, Arany Z. Human cardiac metabolism. *Cell Metab*. 2024;36:1456-1481. doi: 10.1016/j.cmet.2024.06.003
48. Wu Q, Yao Q, Hu T, Yu J, Jiang K, Wan Y, Tang Q. Dapagliflozin protects against chronic heart failure in mice by inhibiting macrophage-mediated inflammation, independent of SGLT2. *Cell Rep Med*. 2023;4:101334. doi: 10.1016/j.xcrm.2023.101334
49. Berger JH, Matsuura TR, Bowman CE, Taing R, Patel J, Lai L, Leone TC, Reagan JD, Haldar SM, Arany Z, et al. SGLT2 Inhibitors Act Independently of SGLT2 to Confer Benefit for HFrEF in Mice. *Circ Res*. 2024;135:632-634. doi: 10.1161/CIRCRESAHA.124.324823
50. Koleini N, Meddeb M, Zhao L, Keykhaei M, Kwon S, Farshidfar F, Hahn VS, Pearce EL, Sharma K, Kass DA. Landscape of glycolytic metabolites and their regulating proteins in myocardium from human heart failure with preserved ejection fraction. *Eur J Heart Fail*. 2024. doi: 10.1002/ejhf.3389
51. Hahn VS, Petucci C, Kim MS, Bedi KC, Jr., Wang H, Mishra S, Koleini N, Yoo EJ, Margulies KB, Arany Z, et al. Myocardial Metabolomics of Human Heart Failure With Preserved Ejection Fraction. *Circulation*. 2023;147:1147-1161. doi: 10.1161/CIRCULATIONAHA.122.061846
52. Sun Q, Guven B, Wagg CS, Almeida de Oliveira A, Silver H, Zhang L, Chen B, Wei K, Ketema EB, Karwi QG, et al. Mitochondrial fatty acid oxidation is the major source of cardiac adenosine triphosphate production in heart failure with preserved ejection fraction. *Cardiovasc Res*. 2024;120:360-371. doi: 10.1093/cvr/cvae006
53. Gibb AA, Hill BG. Metabolic Coordination of Physiological and Pathological Cardiac Remodeling. *Circ Res*. 2018;123:107-128. doi: 10.1161/CIRCRESAHA.118.312017
54. Ritterhoff J, Tian R. Metabolic mechanisms in physiological and pathological cardiac hypertrophy: new paradigms and challenges. *Nat Rev Cardiol*. 2023;20:812-829. doi: 10.1038/s41569-023-00887-x
55. Summer G, Kuhn AR, Munts C, Miranda-Silva D, Leite-Moreira AF, Lourenco AP, Heymans S, Falcao-Pires I, van Bilsen M. A directed network analysis of the cardiome identifies molecular pathways contributing to the development of HFpEF. *J Mol Cell Cardiol*. 2020;144:66-75. doi: 10.1016/j.yjmcc.2020.05.008
56. Hahn VS, Knutsdottir H, Luo X, Bedi K, Margulies KB, Haldar SM, Stolina M, Yin J, Khakoo AY, Vaishnav J, et al. Myocardial Gene Expression Signatures in Human Heart Failure With Preserved Ejection Fraction. *Circulation*. 2021;143:120-134. doi: 10.1161/CIRCULATIONAHA.120.050498
57. Meddeb M, Koleini N, Binek A, Keykhaei M, Darehgazani R, Kwon S, Aboaf C, Margulies KB, Bedi KC, Jr., Lehar M, et al. Myocardial ultrastructure of human

heart failure with preserved ejection fraction. *Nat Cardiovasc Res*. 2024;3:907-914. doi: 10.1038/s44161-024-00516-x

58. Aubert G, Martin OJ, Horton JL, Lai L, Vega RB, Leone TC, Koves T, Gardell SJ, Kruger M, Hoppel CL, et al. The Failing Heart Relies on Ketone Bodies as a Fuel. *Circulation*. 2016;133:698-705. doi: 10.1161/CIRCULATIONAHA.115.017355
59. Murashige D, Jang C, Neinast M, Edwards JJ, Cowan A, Hyman MC, Rabinowitz JD, Frankel DS, Arany Z. Comprehensive quantification of fuel use by the failing and nonfailing human heart. *Science*. 2020;370:364-368. doi: 10.1126/science.abc8861
60. Bedi KC, Jr., Snyder NW, Brandimarto J, Aziz M, Mesaros C, Worth AJ, Wang LL, Javaheri A, Blair IA, Margulies KB, et al. Evidence for Intramyocardial Disruption of Lipid Metabolism and Increased Myocardial Ketone Utilization in Advanced Human Heart Failure. *Circulation*. 2016;133:706-716. doi: 10.1161/CIRCULATIONAHA.115.017545
61. Yurista SR, Matsuura TR, Sillje HHW, Nijholt KT, McDaid KS, Shewale SV, Leone TC, Newman JC, Verdin E, van Veldhuisen DJ, et al. Ketone Ester Treatment Improves Cardiac Function and Reduces Pathologic Remodeling in Preclinical Models of Heart Failure. *Circ Heart Fail*. 2021;14:e007684. doi: 10.1161/CIRCHEARTFAILURE.120.007684
62. Sun H, Olson KC, Gao C, Prosdocimo DA, Zhou M, Wang Z, Jeyaraj D, Youn JY, Ren S, Liu Y, et al. Catabolic Defect of Branched-Chain Amino Acids Promotes Heart Failure. *Circulation*. 2016;133:2038-2049. doi: 10.1161/CIRCULATIONAHA.115.020226
63. Li T, Zhang Z, Kolwicz SC, Jr., Abell L, Roe ND, Kim M, Zhou B, Cao Y, Ritterhoff J, Gu H, et al. Defective Branched-Chain Amino Acid Catabolism Disrupts Glucose Metabolism and Sensitizes the Heart to Ischemia-Reperfusion Injury. *Cell Metab*. 2017;25:374-385. doi: 10.1016/j.cmet.2016.11.005
64. Lopaschuk GD, Karwi QG, Tian R, Wende AR, Abel ED. Cardiac Energy Metabolism in Heart Failure. *Circ Res*. 2021;128:1487-1513. doi: 10.1161/CIRCRESAHA.121.318241
65. Ichihara K, Neely JR, Siehl DL, Morgan HE. Utilization of leucine by working rat heart. *Am J Physiol*. 1980;239:E430-436. doi: 10.1152/ajpendo.1980.239.6.E430
66. Wang W, Zhang F, Xia Y, Zhao S, Yan W, Wang H, Lee Y, Li C, Zhang L, Lian K, et al. Defective branched chain amino acid catabolism contributes to cardiac dysfunction and remodeling following myocardial infarction. *Am J Physiol Heart Circ Physiol*. 2016;311:H1160-H1169. doi: 10.1152/ajpheart.00114.2016
67. Murashige D, Jung JW, Neinast MD, Levin MG, Chu Q, Lambert JP, Garbincius JF, Kim B, Hoshino A, Marti-Pamies I, et al. Extra-cardiac BCAA catabolism lowers blood pressure and protects from heart failure. *Cell Metab*. 2022;34:1749-1764 e1747. doi: 10.1016/j.cmet.2022.09.008
68. Rector TS, Bank AJ, Mullen KA, Tschumperlin LK, Sih R, Pillai K, Kubo SH. Randomized, double-blind, placebo-controlled study of supplemental oral L-arginine in patients with heart failure. *Circulation*. 1996;93:2135-2141. doi: 10.1161/01.cir.93.12.2135
69. Zhou B, Tian R. Mitochondrial dysfunction in pathophysiology of heart failure. *J Clin Invest*. 2018;128:3716-3726. doi: 10.1172/JCI120849

70. Abel ED, Doenst T. Mitochondrial adaptations to physiological vs. pathological cardiac hypertrophy. *Cardiovasc Res*. 2011;90:234-242. doi: 10.1093/cvr/cvr015
71. Kumar AA, Kelly DP, Chirinos JA. Mitochondrial Dysfunction in Heart Failure With Preserved Ejection Fraction. *Circulation*. 2019;139:1435-1450. doi: 10.1161/CIRCULATIONAHA.118.036259
72. Cogliati S, Enriquez JA, Scorrano L. Mitochondrial Cristae: Where Beauty Meets Functionality. *Trends Biochem Sci*. 2016;41:261-273. doi: 10.1016/j.tibs.2016.01.001
73. Hammer S, van der Meer RW, Lamb HJ, Schar M, de Roos A, Smit JW, Romijn JA. Progressive caloric restriction induces dose-dependent changes in myocardial triglyceride content and diastolic function in healthy men. *J Clin Endocrinol Metab*. 2008;93:497-503. doi: 10.1210/jc.2007-2015
74. Wu CK, Tsai HY, Su MM, Wu YF, Hwang JJ, Lin JL, Lin LY, Chen JJ. Evolutional change in epicardial fat and its correlation with myocardial diffuse fibrosis in heart failure patients. *J Clin Lipidol*. 2017;11:1421-1431. doi: 10.1016/j.jacl.2017.08.018
75. Wu CK, Lee JK, Hsu JC, Su MM, Wu YF, Lin TT, Lan CW, Hwang JJ, Lin LY. Myocardial adipose deposition and the development of heart failure with preserved ejection fraction. *Eur J Heart Fail*. 2020;22:445-454. doi: 10.1002/ejhf.1617
76. Benador IY, Veliova M, Mahdaviani K, Petcherski A, Wikstrom JD, Assali EA, Acin-Perez R, Shum M, Oliveira MF, Cinti S, et al. Mitochondria Bound to Lipid Droplets Have Unique Bioenergetics, Composition, and Dynamics that Support Lipid Droplet Expansion. *Cell Metab*. 2018;27:869-885 e866. doi: 10.1016/j.cmet.2018.03.003
77. Wang H, Sreenivasan U, Hu H, Saladino A, Polster BM, Lund LM, Gong DW, Stanley WC, Sztalryd C. Perilipin 5, a lipid droplet-associated protein, provides physical and metabolic linkage to mitochondria. *J Lipid Res*. 2011;52:2159-2168. doi: 10.1194/jlr.M017939
78. Najt CP, Adhikari S, Heden TD, Cui W, Gansemer ER, Rauckhorst AJ, Markowski TW, Higgins L, Kerr EW, Boyum MD, et al. Organelle interactions compartmentalize hepatic fatty acid trafficking and metabolism. *Cell Rep*. 2023;42:112435. doi: 10.1016/j.celrep.2023.112435
79. Kim H, Lee S, Jun Y, Lee C. Structural basis for mitoguardin-2 mediated lipid transport at ER-mitochondrial membrane contact sites. *Nat Commun*. 2022;13:3702. doi: 10.1038/s41467-022-31462-6
80. Zhang Y, Liu X, Bai J, Tian X, Zhao X, Liu W, Duan X, Shang W, Fan HY, Tong C. Mitoguardin Regulates Mitochondrial Fusion through MitoPLD and Is Required for Neuronal Homeostasis. *Mol Cell*. 2016;61:111-124. doi: 10.1016/j.molcel.2015.11.017
81. Wallner M, Eaton DM, Berretta RM, Liesinger L, Schittmayer M, Gindlhuber J, Wu J, Jeong MY, Lin YH, Borghetti G, et al. HDAC inhibition improves cardiopulmonary function in a feline model of diastolic dysfunction. *Sci Transl Med*. 2020;12. doi: 10.1126/scitranslmed.aay7205
82. Scandalis L, Kitzman DW, Nicklas BJ, Lyles M, Brubaker P, Nelson MB, Gordon M, Stone J, Bergstrom J, Neufer PD, et al. Skeletal Muscle Mitochondrial

Respiration and Exercise Intolerance in Patients With Heart Failure With Preserved Ejection Fraction. *JAMA Cardiol*. 2023;8:575-584. doi: 10.1001/jamacardio.2023.0957

83. Strocchi S, Liu L, Wang R, Haseli SP, Capone F, Bode D, Nambiar N, Eroglu T, Santiago Padilla L, Farrelly C, et al. Systems Biology Approach Uncovers Candidates for Liver-Heart Interorgan Crosstalk in HFpEF. *Circ Res*. 2024. doi: 10.1161/CIRCRESAHA.124.324829

FIGURE LEGENDS

Fig. 1: Clinical manifestations of HFpEF are observed in the ZSF1-Obese rat. Physiological characterization of HFpEF. (**A**) Schematic of study design. (**B**) Body weights of WKY (control), Lean (Hypertensive; HTN), and ZSF1-Obese (Metabolic Syndrome + HTN; HFpEF) rats. (**C**) Assessment of systolic (SBP) and diastolic (DBP) blood pressure obtained during invasive hemodynamics. (**D**) Distance run during a treadmill exercise capacity test. (**E**) Indices of cardiac left ventricular diastolic function assessed by echocardiography for the E/e' ratio and invasive hemodynamics for the left ventricular end diastolic pressure (LVEDP). (**F**) Determination of cardiac systolic function assessed by the echocardiography for the left ventricular ejection fraction (LVEF%). (**G**) Gravimetric assessment of left ventricle and left atria normalized to tibia length (TL). n = 4-7 male rats per group, mean ± SEM. One-way ANOVA with Holm-Sidak's post-hoc test, *p ≤ 0.05, **p ≤ 0.01, ***p ≤ 0.001, ****p ≤ 0.0001.

Fig. 2: Hypertension significantly impacts the cardiac metabolome with minimal impact on the transcriptome. RNAseq and metabolomic comparisons of hearts from Lean vs WKY control rats. (**A**) Summary of the upregulated and downregulated transcriptional and metabolic changes. Gene ontology analysis revealing the top upregulated (**B**) biological processes and (**C**) KEGG pathways of those genes found to be differentially expressed. Gene ontology analysis revealing the top downregulated (**D**) biological processes and (**E**) KEGG pathways of those genes found to be differentially expressed. (**F**) Pathway enrichment analysis of the cardiac metabolome indicated those pathways found to be most significantly affected in ZSF1 rats due to hypertension. Fold

change cutoffs of ≥ 2.0 (RNAseq) and ≥ 1.25 (metabolomics) were employed with an FDR ≤ 0.05. n = 6 male rats per group for RNAseq and n = 7 male rats per group for metabolomics. FDR = false discovery rate.

Fig. 3: Transcriptional cardiac remodeling is dependent upon the two hits of obesity and hypertension in ZSF1-Obese HFpEF rats. RNAseq and metabolomic comparisons of hearts from ZSF1-Obese vs Lean rats. (**A**) Summary of the upregulated and downregulated transcriptional and metabolic changes. Gene ontology analysis revealing the top upregulated (**B**) biological processes and (**C**) KEGG pathways of those genes found to be differentially expressed. Gene ontology analysis revealing the top downregulated (**D**) biological processes and (**E**) KEGG pathways of those genes found to be differentially expressed. (**F**) Pathway enrichment analysis of the cardiac metabolome indicated those pathways found to be most significantly affected in ZSF1 rats due to hypertension. Fold change cutoffs of ≥ 2.0 (RNAseq) and ≥ 1.25 (metabolomics) were employed with an FDR ≤ 0.05. n = 6 male rats per group for RNAseq and n = 7 male Lean and 8 male ZSF1-Obese rats for metabolomics. FDR = false discovery rate.

Fig. 4: Integrated network analysis of RNAseq and metabolomic dataset reveals unique metabolic pathways impacted in HFpEF. Integrated analysis of cardiac omics datasets to identify those pathways most impacted by transcriptional and metabolic remodeling due to (**A**) hypertensive phenotype (Lean vs WKY) or (**B**) the observed HFpEF phenotype (ZSF1-Obese vs Lean). Fold change cutoffs of ≥ 2.0 (RNAseq) and ≥

1196 1.25 (metabolomics) were employed with an FDR ≤ 0.05. A greater pathway impact
1197 indicates a greater influence at the transcriptional and metabolic level to a given
1198 pathway. Labeled pathways had a *p*-value ≤ 0.05. n = 6 male rats per group for RNAseq
1199 and n = 7 male Lean and 8 male ZSF1-Obese rats for metabolomics. FDR = false
1200 discovery rate.
1201
1202 **Fig. 5: HFpEF results in the transcriptional and metabolic downregulation of**
1203 **pathways central to energy metabolism.** Pathway maps of the transcriptional and
1204 metabolic alterations in Lean vs WKY and ZSF1-Obese vs Lean rats in energy
1205 generating pathways, specifically (**A**) aerobic glycolysis, (**B**) fatty acid oxidiation, (**C**)
1206 and the Krebs cycle. Additional pathways indicated in boxes provide an objective
1207 summary of the transcriptional and metabolic increase or decrease observed. Genes
1208 and metabolites significantly **increased** or **decreased** in expression or abundance (Fold
1209 change ≥ 2.0 (RNAseq) and ≥ 1.25 (metabolomics); FDR ≤ 0.05) are as indicated.
1210
1211 **Fig. 6: Mitochondrial ultrastructural remodeling in the HFpEF heart is**
1212 **characterized by a decrease in mitochondrial content, cristae disorganization,**
1213 **and lipid droplet association.** Transmission electron micrographs of cardiomyocyte
1214 mitochondrial and lipid droplet (LD) ultrastructure. (**A**) Representative images of WKY,
1215 Lean, and ZSF1-Obese cardiomyocyte ultrastructure indicating cristae disorganization
1216 (**yellow arrows**) and lipid droplet accumulation and interaction with mitochondria (**red**
1217 **arrows**). (**B**) mitochondrial area (i.e., content) quantified by the number of mitochondria
1218 per image area and the percent area of mitochondria to total area. (**C**) Mitochondrial

shape quantified by the Feret's diameter and circularity index. (**D**) Quantification of LD area (i.e., content) quantified by the number of LDs per image area and the percent area of LDs to total area. (**E**) LD shape quantified by the Feret's diameter and circularity index. (**F**) Analysis of mitochondrial-LD interaction quantified by the number of mito-LD contacts per image area, the outer mitochondrial membrane (OMM) perimeter in contact with an LD, and the LD perimeter in association with the OMM. (**G**) Determination of sarcomeric length measured from z-line to z-line. n = 4 male rats per group, , mean ± SEM. One-way ANOVA with Holm-Sidak's post-hoc test, *p ≤ 0.05, **p ≤ 0.01, ***p ≤ 0.001, ****p ≤ 0.0001.

Fig. 7: Mitochondrial dysfunction characterized by impaired respiratory activity and disrupted calcium handling is a key feature of the HFpEF heart. Functional assessment of the mitochondrial function in the HFpEF heart. (**A**) Determination of mitochondrial content assessed by citrate synthase activity. Interrogation of mitochondrial respiratory function by assessing oxygen consumption rates (OCR) of (**B,C**) complex I (pyruvate + malate)-specific substrates, (**D,E**) complex II (succinate)-specific substrate + rotenone (complex I inhibitor), and (**F,G**) fatty acid oxidation capacity (palmitoyl-L-carnitine): state 3 (substrate-mediated) oxygen consumption and the respiratory control ratio (RCR) providing an index of oxygen consumption to ATP-production coupling. (**H,I**) Mitochondrial calcium uptake in response to repeated 2.5 µM boluses. Mitochondrial swelling in response to a 500 µM bolus, displayed as both (**J**) uncorrected and (**K**) normalized prior to calcium addition. Quantification of mitochondrial swelling indicated by (**L**) percent change to WKY baseline and (**M**) area above the

curve. Immunoblotting of (**N**) VDAC1/3 and components of the mitochondrial calcium uniporter and (**O**) subunits of ETC complexes. Proteins differentially expressed in protein abundance are indicated in **red**. n = 5 male rats per group (A-G), n = 4 male rats per group (I-O), mean ± SEM. One-way ANOVA with Holm-Sidak's post-hoc test, *p ≤ 0.05, ***p ≤ 0.001, ****p ≤ 0.0001.

Figure 1

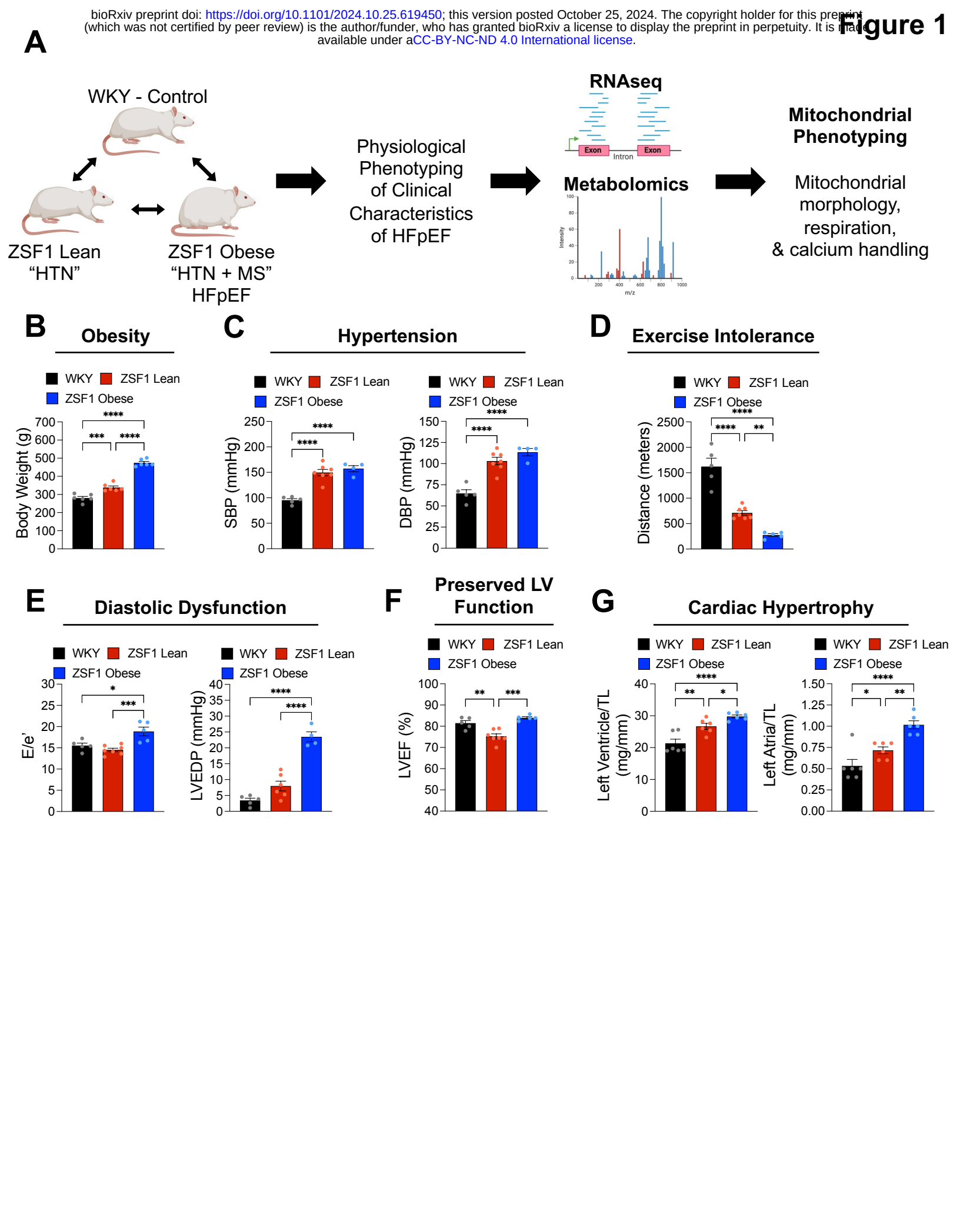

Figure 2

A

Statistical Comparison	
ZSF1 Lean vs WKY	
Transcriptomics	
Total Genes FC≥2.0 FDR≤0.05	233
Genes/Transcripts (↑|↓)	149 | 84
Metabolomics	
Total Biochemicals FC≥1.25 FDR≤0.05	205
Biochemicals (↑|↓)	120 | 85

B

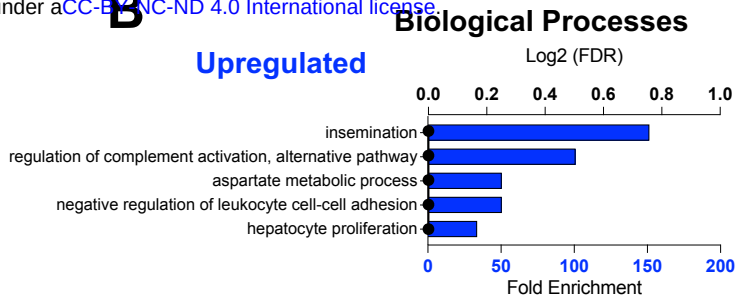

C

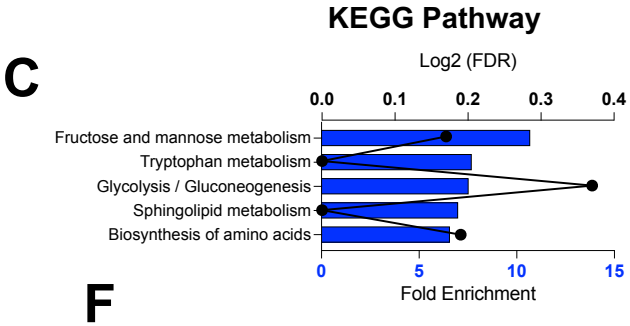

D

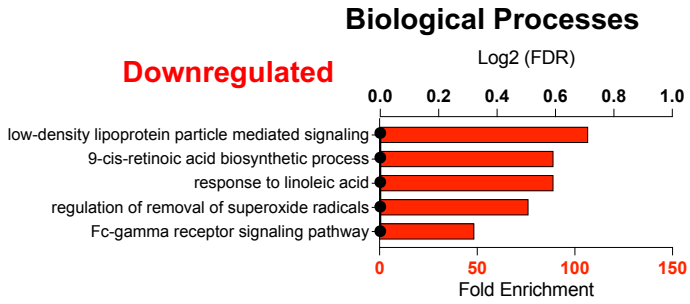

E

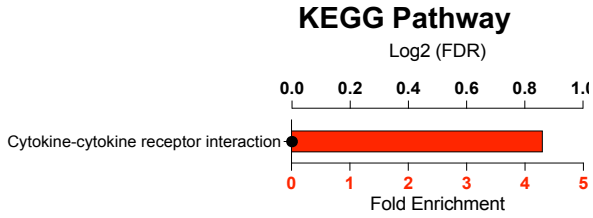

F

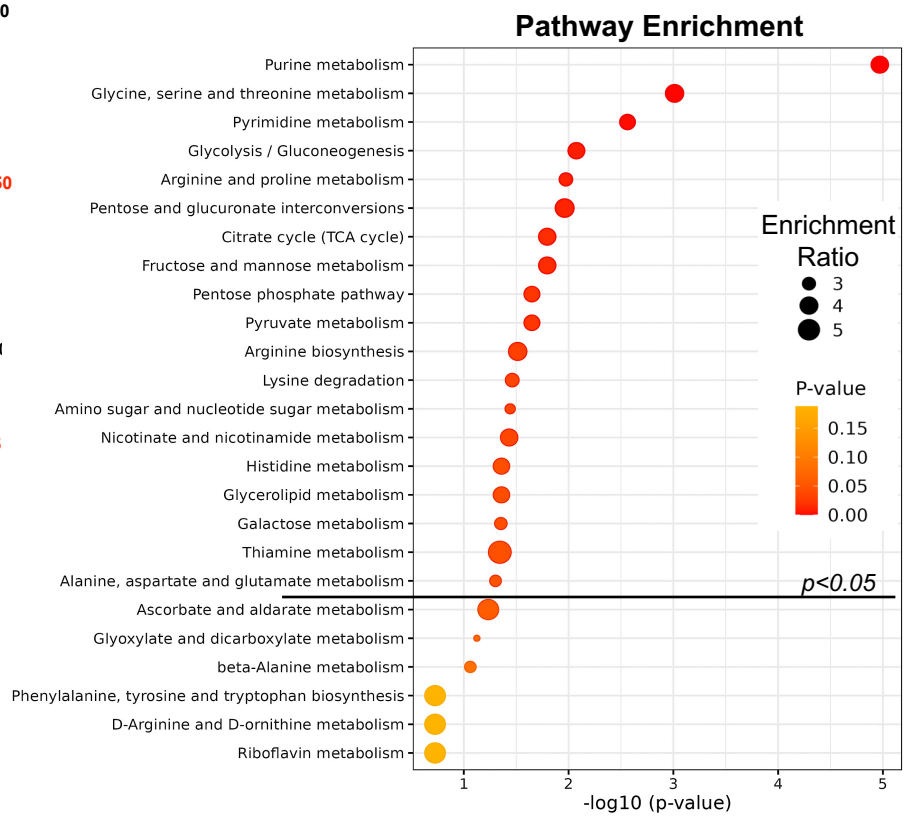

Figure 3

A

Statistical Comparison	
ZSF1 Obese vs ZSF1-Lean	
Transcriptomics	
Total Genes FC≥2.0 FDR≤0.05	5691
Genes/Transcripts (↑|↓)	3123 | 2568
Metabolomics	
Total Biochemicals FC≥1.25 FDR≤0.05	278
Biochemicals (↑|↓)	148 | 130

B

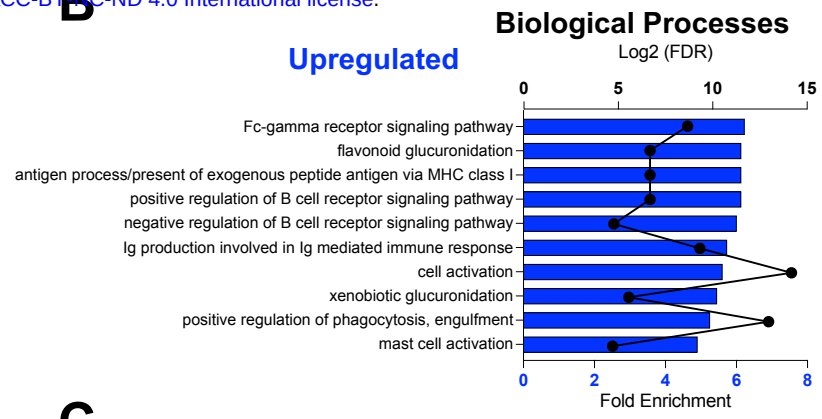

C

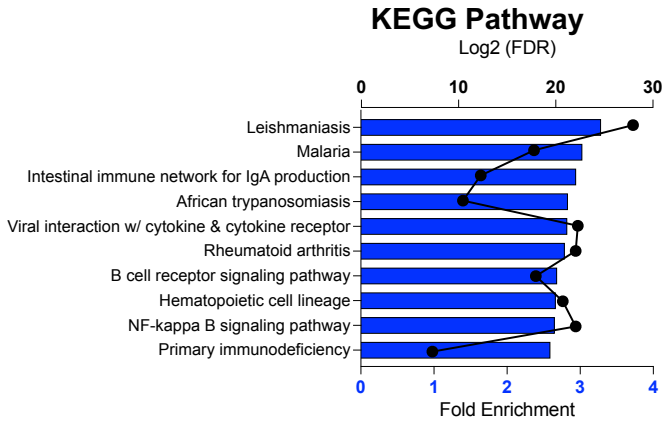

D

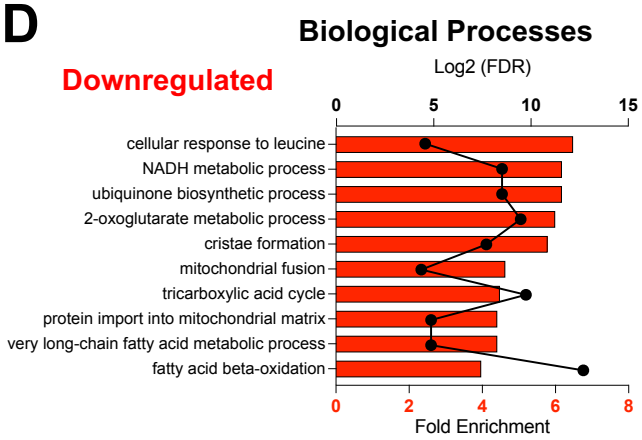

E

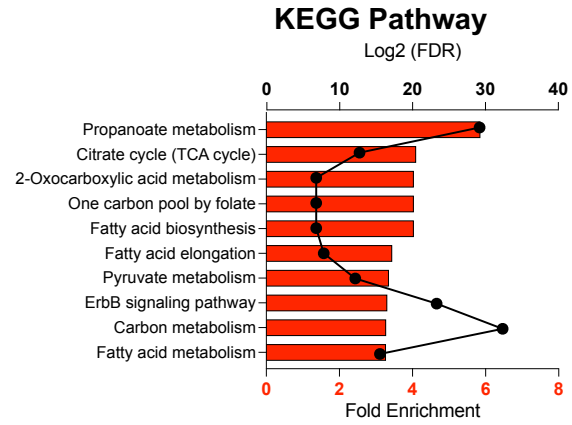

F

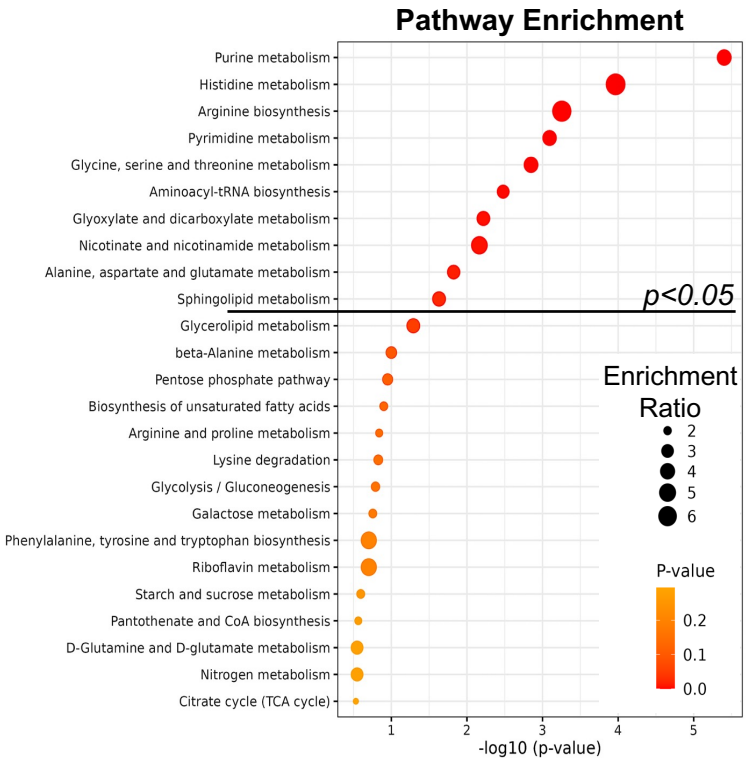

Figure 4

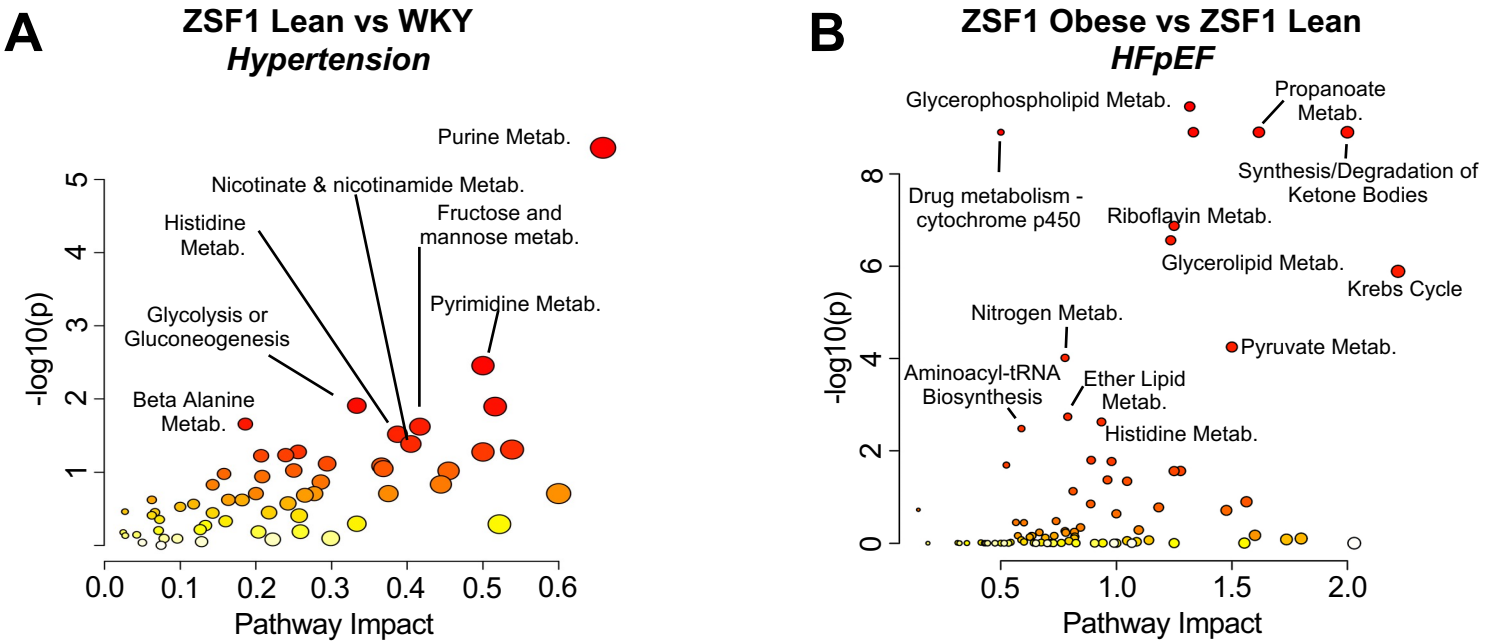

Figure 5

A

ZSF1 Lean vs WKY
Hypertension

ZSF1 Obese vs ZSF1 Lean
HFpEF

Aerobic Glycolysis

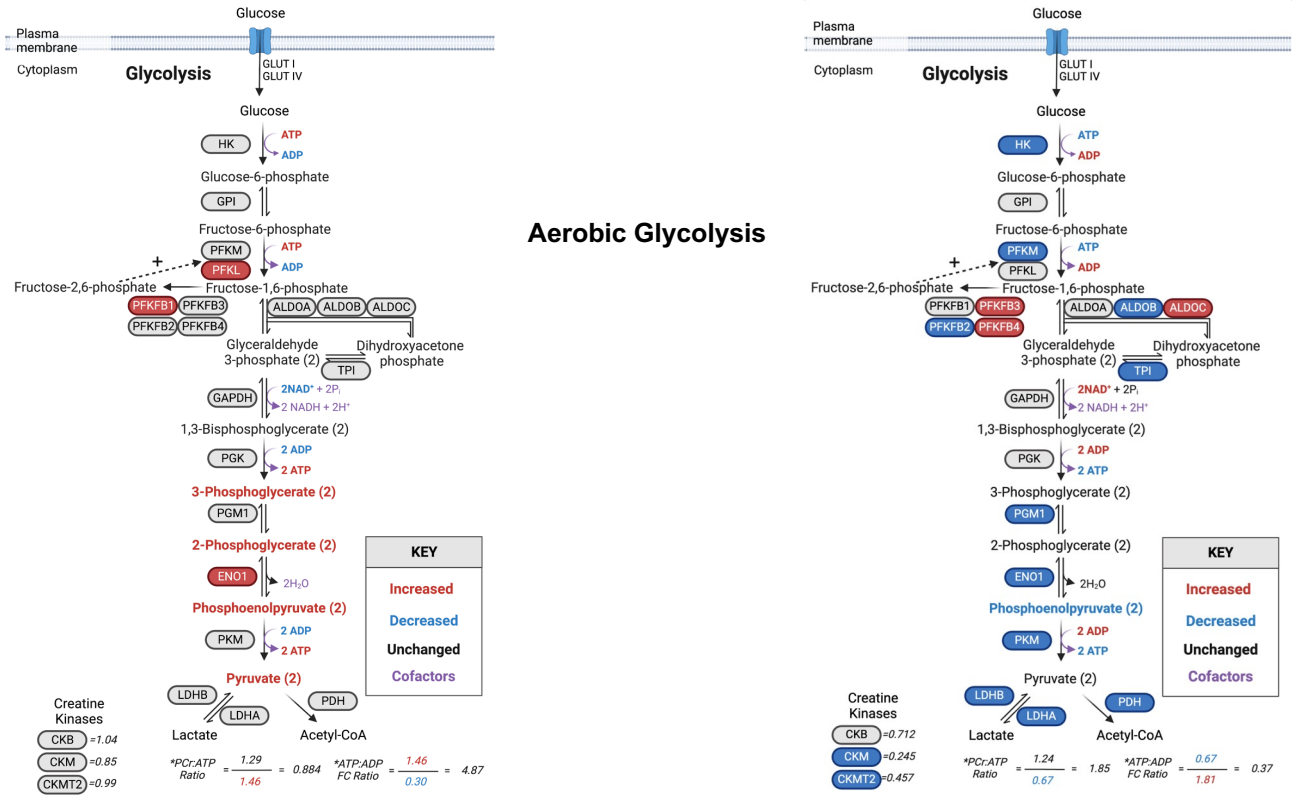

B

Fatty Acid β-oxidation

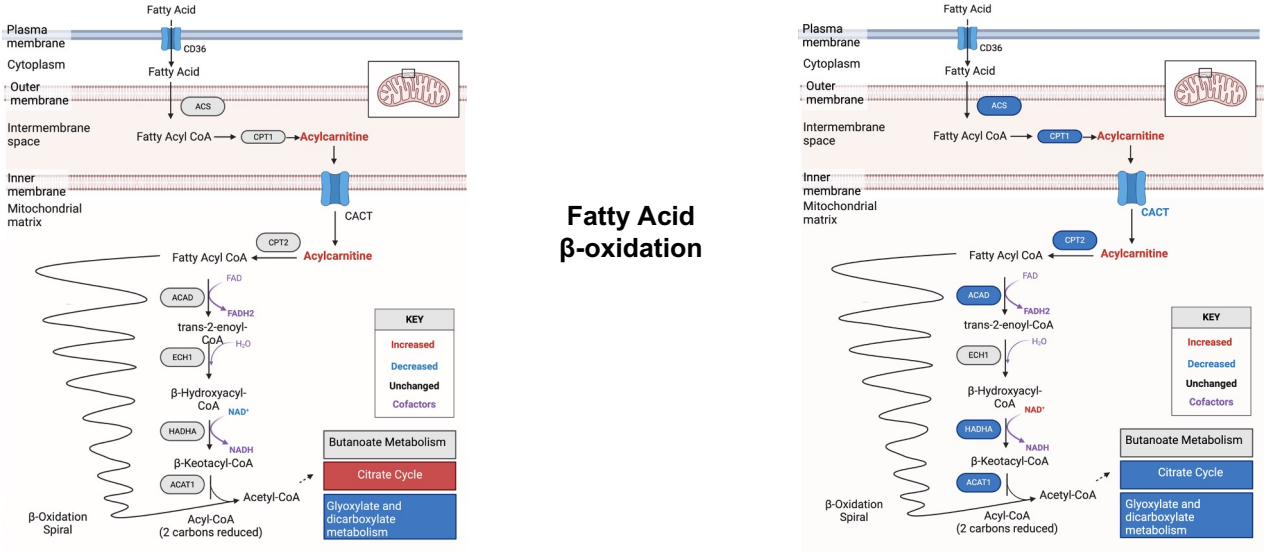

C

Krebs Cycle & Input Pathways

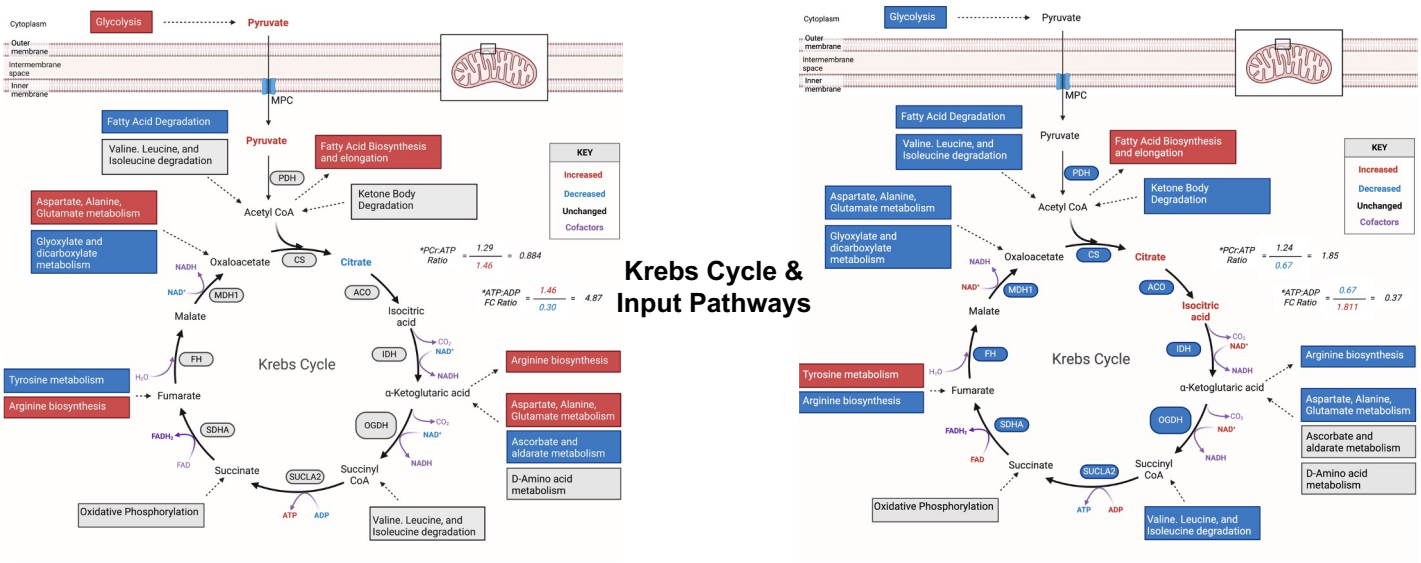

Figure 6

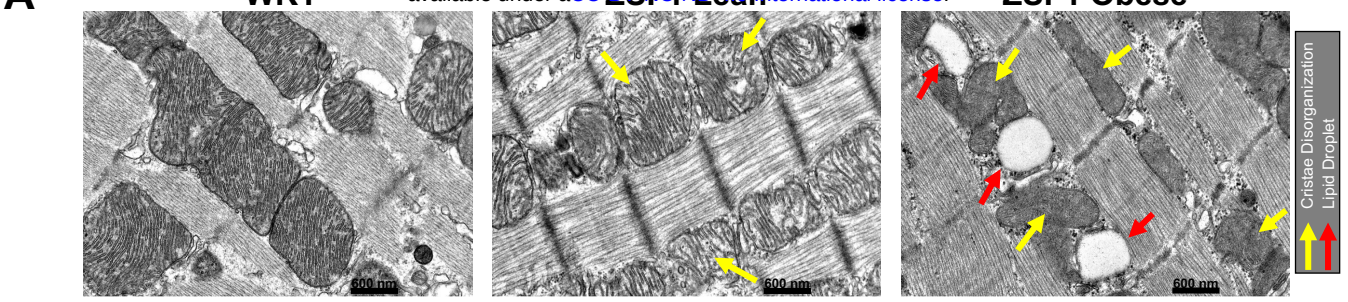

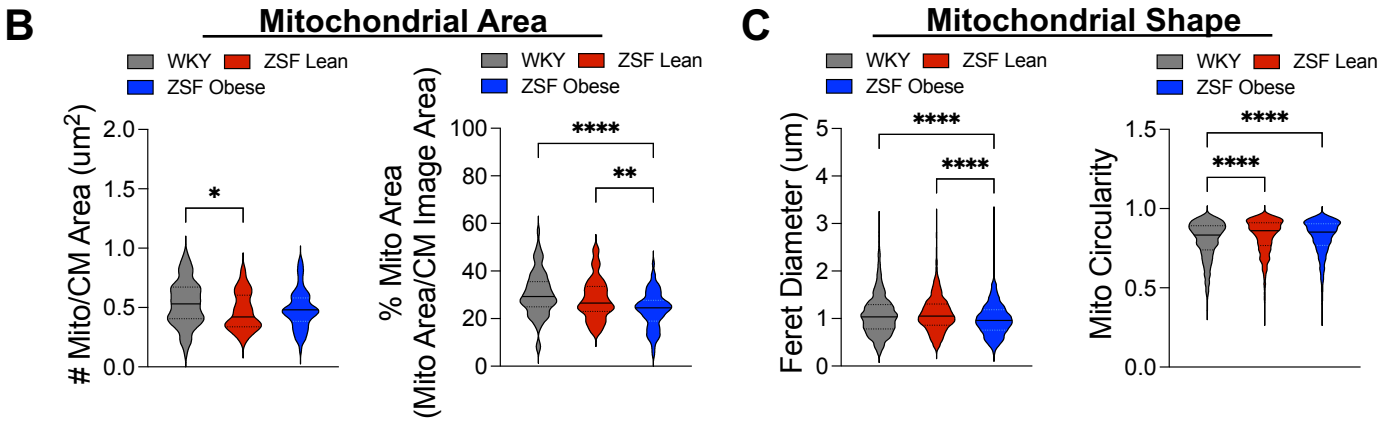

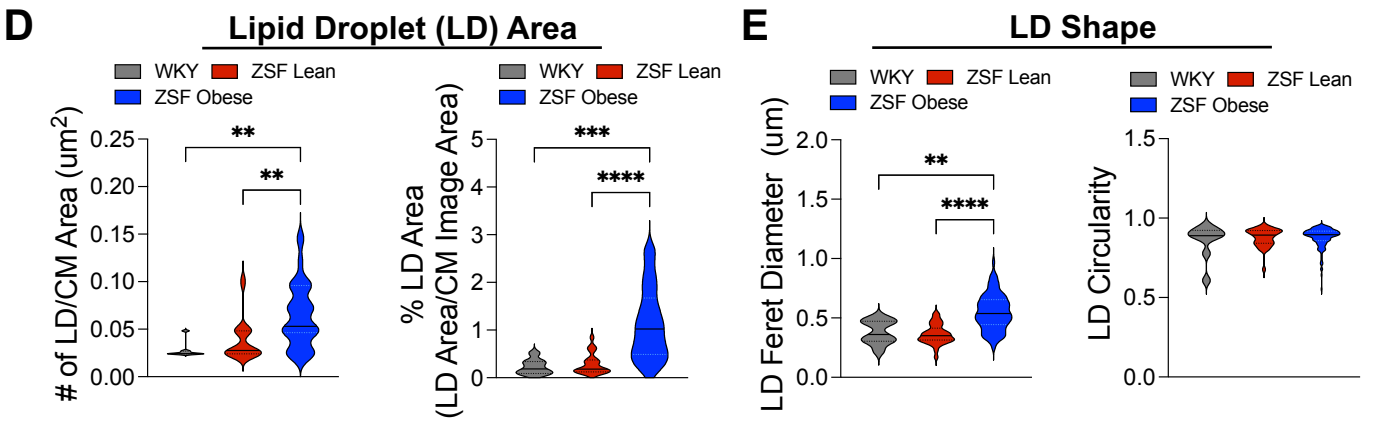

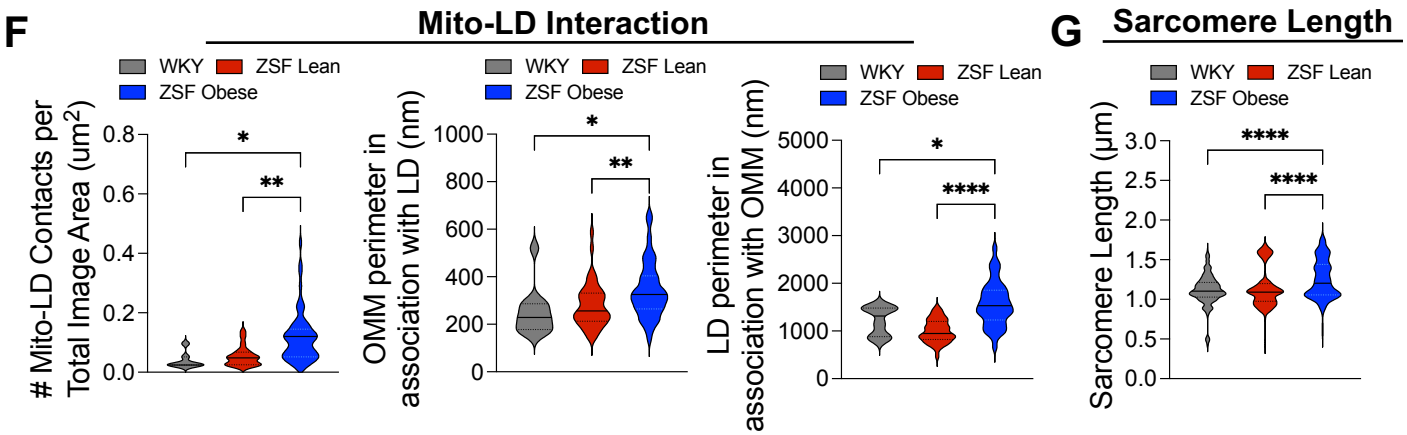

Figure 7